RESEARCH

Knocking out *Fkbp51* decreases CCl$_4$-induced liver injury through enhancement of mitochondrial function and Parkin activity

Bin Qiu[5,7†], Zhaohui Zhong[6†], Longyu Dou[5], Yuxue Xu[5], Yi Zou[8], Korri Weldon[8], Jun Wang[5], Lingling Zhang[5], Ming Liu[5], Kent E. Williams[1], John Paul Spence[3], Richard L. Bell[4], Zhao Lai[8], Weidong Yong[2,5*] and Tiebing Liang[1*]

Abstract

Background and aims Previously, we found that FK506 binding protein 51 (*Fkbp51*) knockout (KO) mice resist high fat diet-induced fatty liver and alcohol-induced liver injury. The aim of this research is to identify the mechanism of *Fkbp51* in liver injury.

Methods Carbon tetrachloride (CCl$_4$)-induced liver injury was compared between *Fkbp51* KO and wild type (WT) mice. Step-wise and in-depth analyses were applied, including liver histology, biochemistry, RNA-Seq, mitochondrial respiration, electron microscopy, and molecular assessments. The selective FKBP51 inhibitor (SAFit2) was tested as a potential treatment to ameliorate liver injury.

Results *Fkbp51* knockout mice exhibited protection against liver injury, as evidenced by liver histology, reduced fibrosis-associated markers and lower serum liver enzyme levels. RNA-seq identified differentially expressed genes and involved pathways, such as fibrogenesis, inflammation, mitochondria, and oxidative metabolism pathways and predicted the interaction of FKBP51, Parkin, and HSP90. Cellular studies supported co-localization of Parkin and FKBP51 in the mitochondrial network, and Parkin was shown to be expressed higher in the liver of KO mice at baseline and after liver injury relative to WT. Further functional analysis identified that KO mice exhibited increased ATP production and enhanced mitochondrial respiration. KO mice have increased mitochondrial size, increased autophagy/mitophagy and mitochondrial-derived vesicles (MDV), and reduced reactive oxygen species (ROS) production, which supports enhancement of mitochondrial quality control (MQC). Application of SAFit2, an FKBP51 inhibitor, reduced the effects of CCl$_4$-induced liver injury and was associated with increased Parkin, pAKT, and ATP production.

Conclusions Downregulation of FKBP51 represents a promising therapeutic target for liver disease treatment.

Keywords FK506binding protein 5/Fkbp51, RNA-seq, Mitochondrial quality control (MQC), SAFit2, Liver disease treatment

---

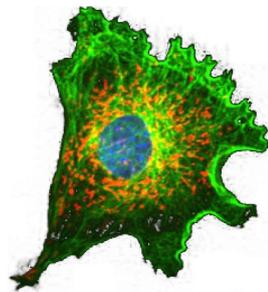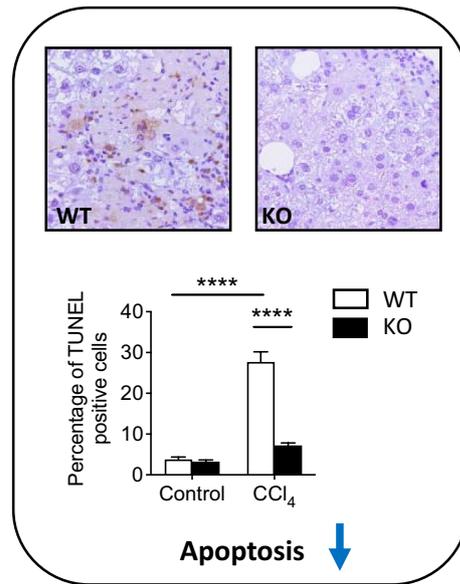†Bin Qiu and Zhaohui Zhong have contributed equally to this work.
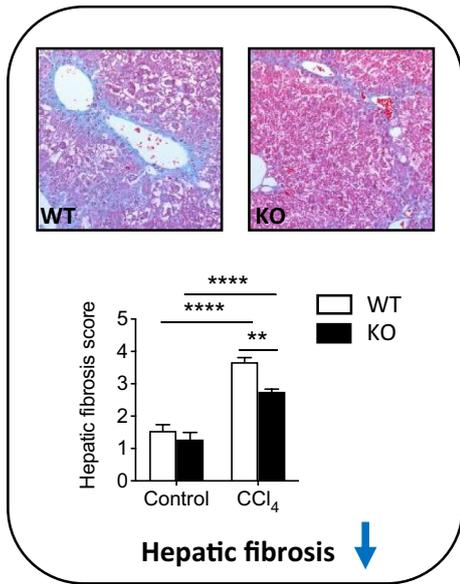
*Correspondence:
Weidong Yong
yongwd@hotmail.com
Tiebing Liang
tliang@iu.edu
Full list of author information is available at the end of the article

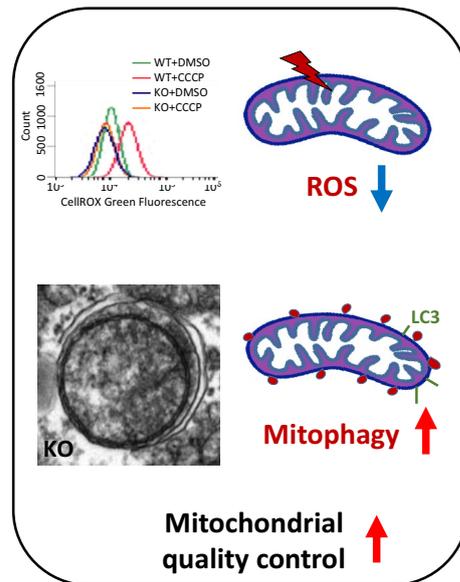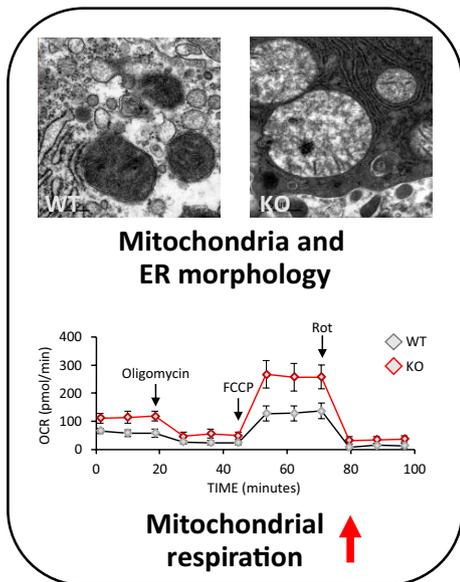Qiu *et al. Cell & Bioscience*   (2024) 14:1

Page 2 of 25

Graphical Abstract

Introduction

Liver diseases are chronic conditions, affecting more than 100 million people worldwide, which can result from obesity, alcohol consumption, viral infection, and toxic-metabolic insults [1]. The subsequent development of cirrhosis increases the risk of hepatocellular carcinoma (HCC), and no effective treatments currently exist to reverse advanced liver disease-associated phenotypes. Thus, early interventions to reduce liver damage and halt further liver disease progression are necessary. As patients with liver disease often present with dysfunction in mitochondrial ultrastructure, dynamics, activity in respiratory chain complexes, and adenosine triphosphate (ATP) synthesis, improving mitochondrial function is one promising strategy to treat chronic liver diseases [2–4].

FK506 binding protein 51 (FKBP51), well known as a glucocorticoid receptor (GR) binding protein, is an essential chaperone of heat-shock protein 90 (HSP90) that affects hypothalamus–pituitary–adrenal (HPA)-axis function in response to stress, regulates protein post-translational modification, and participates in the function of protein signaling pathways [5–9]. Previous studies have shown that FKBP51 plays key roles in metabolic function regulation [10–12]. We have shown that high fat diet-fed *Fkbp51* knockout (KO) mice are resistant to weight gain, hepatic steatosis, and adiposity, and that these effects are correlated with increased energy expenditure [13]. FKBP51 also acts as a chaperone of Akt and affects GRα and PPARγ phosphorylation, and its ablation reduces lipid accumulation and decreases the expression of adipogenic genes [14, 15]. In vitro modeling of hypoxic stress demonstrated that loss of FKBP51 inhibits adipocyte differentiation [16], and others found that maternal nutrient restriction increases the signaling of hypoxia-inducible pathways, including FKBP51, in fetal mouse liver [17]. Furthermore, the loss of *Fkbp51* was demonstrated to ameliorate alcohol-induced liver injury [18]. FKBP51 plays critical roles in hormone nuclear translocation and protein folding [19]. Studies have demonstrated co-localization of FKBP51 with mitochondria and have noted nuclear-mitochondrial shuttling of the protein; a mechanism triggered in response to oxidative stress, adipogenesis, and viral infection [9, 20, 21]. Mitochondrial reactive oxygen species (ROS)-mediated metabolic pathway alterations, and higher levels of ROS generally are known to enhance liver disease progression [11, 15, 22, 23]. However, the role of FKBP51 in mitochondrial function in response to drug-induced liver injury has not been fully elucidated.

Mitochondrial quality control (MQC) is vital in pathophysiological states, supporting nutrient recycling, toxin degradation, and energy regeneration, and its dysfunction is a feature of both alcoholic liver disease (ALD) and non-alcoholic fatty liver disease (NAFLD) [24]. MQC maintains mitochondrial structural integrity, including the removal of portions of damaged mitochondria through mitochondrial-derived vesicles (MDVs), and regulates mitochondrial biogenesis through fission and fusion [25, 26]. Autophagy is another mechanism employed to adapt to liver injury induced by carbon tetrachloride (CCl_4) [27, 28]. A network of proteases and chaperones are involved at different molecular levels of MQC. One well-studied participant in MQC is Parkin, which functions in regulating misfolded protein degradation via the ubiquitin–proteasome system, the shedding of vesicles via interaction with PTEN Induced Kinase 1 (PINK1) [29], and mitophagy through triggering the polyubiquitination of mitochondrial membrane proteins and proteasomal activation [26].

In this study, we applied the widely used CCl_4-induced liver injury model with modification [30, 31] and showed that *Fkbp51* KO mice were protected against liver injury as evidenced by liver histology, fibrogenesis markers, and serum liver enzymes. RNA-seq pointed to the enrichment of mitochondrial function-related pathways, particularly an increase in Parkin expression. We further examined mitochondrial morphology, ATP production, and MQC-related changes, and revealed that loss of FKBP51 enhances mitochondrial function. Application of SAFit2, a selective inhibitor of FKBP51, demonstrated the potential of targeting FKBP51 in liver injury treatment. Thus, downregulation of FKBP51 activity and a subsequent increase in Parkin and MQC activity is a potential therapeutic approach for the treatment of liver disease. These findings shed new light on FKBP51 with strong implications for its role in the regulation of liver damage via Parkin-associated mitochondrial regulation.

Results

Elimination of *Fkbp51* ameliorates CCl_4-induced liver injury

In order to investigate the involvement of FKBP51 in liver injury, wildtype (WT) and knockout (KO) mice were subjected to CCl_4 treatment three times per week for a duration of 2 weeks. For the purpose of comparing and analyzing the gross liver phenotype among the groups, the livers were removed from the mice without undergoing perfusion. In the WT mouse liver, CCl_4 treatment resulted in a robust color change, rough surface, and stiffness with multiple fibrotic nodules (Fig. 1a, arrows). However, the CCl_4-treated livers of KO mice exhibited fewer of these pathophysiological phenotypes, suggesting a protective effect of *Fkbp51* KO (Fig. 1a). Serum levels of aspartate transaminase (AST) and alanine aminotransferase (ALT) (Fig. 1b, c), which were low at baseline, were significantly more elevated in WT mice than in KO
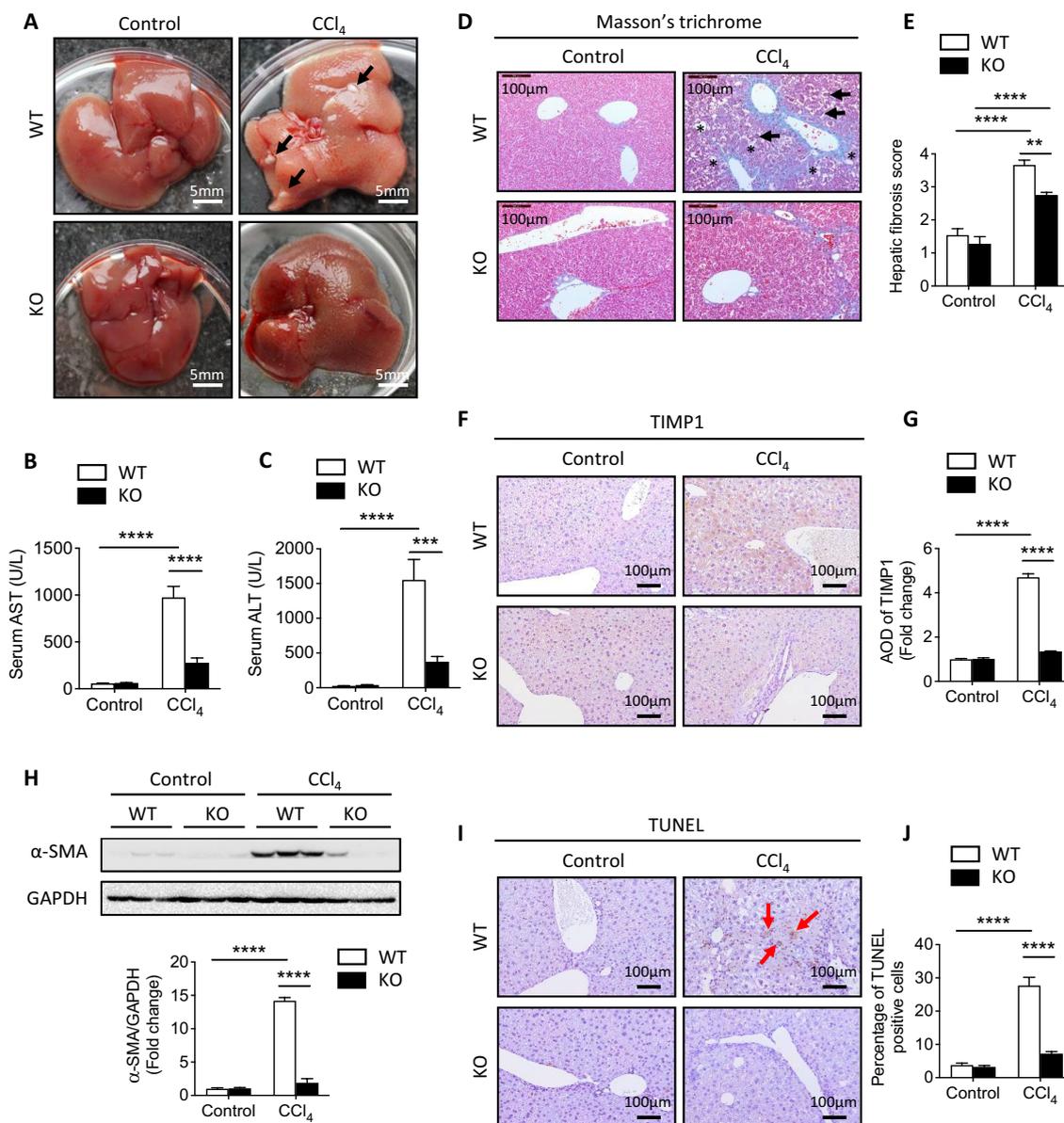
Fig. 1 Ablation of *Fkbp51* gene reduces CCl_4-induced liver damage. **A** Gross liver structure was observed in control and CCl_4-treated *Fkbp51* KO and WT littermate mice. In WT liver with CCl_4 treatment, the fibrosis nodules are indicated by black arrows. **B**, **C** Serum analyses of Control and CCl_4-treated *Fkbp51* KO and WT were performed to determine the concentrations of AST and ALT. **D** Histological examination of Control and CCl_4-treated *Fkbp51* KO and WT liver sections stained with Masson's trichrome. Mice treated with CCl_4 displayed portal vein fibrosis and ballooning (star), and hepatocytes undergoing necrosis (arrow). **E** CCl_4-treated WT liver sections possess significantly higher hepatic fibrosis scores as compared to *Fkbp51* KO liver. **F** Expression patterns of TIMP1 detected by IHC are higher in the liver sections of CCl_4-treated WT mice relative to KO mice. **G** Quantitation of AOD of TIMP1 in liver sections. **H**. Immunoblot and quantification showed less α-SMA protein in CCl_4-treated KO than WT. **I** TUNEL was performed to measure apoptosis in the liver. More apoptotic cells (indicated by arrows) were found following CCl_4 treatment in WT than KO liver. **J** Quantitation of percentage TUNEL-positive hepatocytes (%) in liver sections. Graphs represent mean values ± SEM from 10 mice for each group. *p* values were determined by two-way ANOVA with the statistical significance labeled as follows: ** as $p < 0.01$, *** as $p < 0.001$ and **** as $p < 0.0001$. Key: WT, wild type; KO, *Fkbp51* KO; AOD, average optical density

following CCl_4 treatment (Fig. 1b, c), indicating less liver damage in the KO mouse group.

Masson's trichrome staining (Fig. 1d) was used to evaluate histopathologic alterations in the tissue. Both WT and KO livers in the control group contained cells possessing a normal morphology and regular collagen distribution. After CCl_4 treatment however, ballooning (*), hepatocellular necrosis (arrows), and extensive collagen

deposition, were observed in WT mice (Fig. 1d, CCl$_4$ panel). Notably, collagen bundles surrounding hepatic nodules were significantly attenuated in KO mice when compared to WT mice (Fig. 1d). The grade of liver fibrosis was scored following published guidelines and was shown to be significantly lower in KO mice relative to WT mice following CCl$_4$ treatment ($P < 0.0001$) with no differences observed at baseline (Fig. 1e) [32]. Consistent with these findings, immunohistochemical (IHC) labeling showed that hepatic collagen I deposition was much lower in KO relative to WT mice after CCl$_4$ treatment (Additional file 2: Fig. S1A). Other fibrogenesis-associated markers upregulated to a greater degree in WT mice after CCl$_4$ injection included tissue inhibitor of metalloproteinase 1 (TIMP-1) (Fig. 1f, g) and connective tissue growth factor (CTGF) (Additional file 2: Fig. S1B). Alpha smooth muscle actin (α-SMA), a marker of hepatic stellate cell (HSC) activation, was also expressed at higher levels in CCl$_4$-injured WT liver than in KO as measured by western blotting and IHC labeling (Fig. 1h and Additional file 2: Fig. S1C). These data indicate that KO mice are less susceptible to CCl$_4$-induced liver injury-related fibrosis, matrix remodeling, and HSC activation relative to WT mice. Additionally, more apoptotic cells (arrows), a key feature of liver injury, were found in CCl$_4$-treated WT mice compared to KO mice as determined by terminal deoxynucleotidyl transferase deoxyuridine triphosphate nick end labeling (TUNEL) (Fig. 1i, j). The observed morphological and cellular maker alterations demonstrate that loss of *Fkbp51* confers protection from hepatic injury.

RNA transcriptome profiling identifies pathways and genes important to liver and mitochondrial function

RNA-seq was applied to profile gene expression differences in the livers of KO and WT mice with or without CCl$_4$ treatment. Pairwise comparisons identified differentially expressed genes (DEGs). Using a fold change cut off > 2.0 and an adjusted *p*-value (adj *p*) of < 0.05, the number of DEGs were determined between KO and WT

for either CCl$_4$ injection (745 genes), control solvent (105 genes), or both (48 genes) (Fig. 2a). The 745 unique DEGs between KO and WT for CCl$_4$ treatment became our main interest and were used as input for ingenuity pathway analysis (IPA). The bar-chart represents the most significant pathways altered between KO and WT mice after CCl$_4$ injury (Fig. 2b). Among those, we observed significant differences in pathways relevant to liver function demonstrating a distinctive response to CCl$_4$ injury in *Fkbp51* KO mice. Such pathways included lipopolysaccharides (LPS)/interleukin 1 (IL-1)-mediated inhibition of retinoid X receptor (RXR), hepatic fibrosis/HSC activation, liver X receptor (LXR)/RXR activation, and fatty acid β-oxidation I. Molecules of interest in the IPA pathway are included in Additional file 1: Table S1. Similarly, the identified Kyoto encyclopedia of genes and genomes (KEGG) pathways and involved proteins suggested the PPAR signaling pathway and many others are significantly different between KO and WT mice (Table 1). These signaling pathways directly regulate liver function and are well established in the progression of liver disease pathology, further supporting a critical role of *Fkpb51* in liver injury response [33].

Regulator effects analysis featuring the top predicted upstream regulators were plotted by their activation Z-score (Fig. 2c). Immuno-responsive substances (LPS, transforming growth factor β1 (TGF-β1), and the inactivation of IL-6 and IL-1B in KO mice indicate a decreased liver inflammatory response (Fig. 2c). We also measured immune factors and consistently found lower levels of interferon γ (IFN-γ), IL-6, TGF-β1, and nuclear factor-κB (NFκB) in KO mice relative to WT mice at baseline (Additional file 2: Fig. S2A–D). Following treatment with CCl$_4$, the levels of these factors remained significantly lower in KO mice compared to WT (Additional file 2: Fig. S2A–D). The levels of IL-10 and tumor necrosis factor α (TNF-α) were similar between KO and WT mice at baseline but were lower in KO mice compared to WT mice after CCl$_4$ injury (Additional file 2: Fig. S2E, F). Additionally, hormone regulators [Medrol, dihydrotestosterone

---

(See figure on next page.)

Fig. 2 RNA-Seq reveals differentially expressed genes (DEGs), downstream effects, and upstream regulators in Control and CCl$_4$-treated *Fkbp51* KO and WT liver samples. **A** Venn Diagram shows differentially expressed genes (DEGs) between CCl$_4$-treated *Fkbp51* KO and WT, between vehicle control-treated *Fkbp51* KO and WT, and in common of both conditions. Statistical significance was set as the adjusted *p*-value (adj *p*) < 0.05 and fold change > = 2. **B** The bar-chart represents downstream effects, and the most significant canonical pathways are plotted by their statistical significance (-log *p*-value) when unique CCl$_4$-responsive DEGs served as the input for IPA pathway analysis. **C** Regulator effects analysis featuring the top predicted upstream regulators were plotted by their activation Z-score. Immuno-responsive substances (LPS, TGF-β1, IL-6, and IL-1B), hormone regulators (Medrol, DHT, and LEP), ᴅ-glucose, and CCl$_4$ are inhibited, while functional enzymes related to fatty acid β-oxidation (ACOX1), ligand-binding receptors (AHR), and nuclear factors (PPARγ) are activated. **D** STRING analysis identified clusters of down- and upregulated genes with log2FC KO/WT higher than 2 involved in several critical functions of liver fibrosis formation. Arrows indicate up- and downregulation and the fold changes are listed. (*Abbreviations*: ACOX1, Acyl-CoA Oxidase 1; AHR, Aryl Hydrocarbon Receptor; DHT, dihydrotestosterone; LEP, leptin; LPS, lipopolysaccharide; Medrol, methylprednisolone. Key: WT, wild type; KO, *Fkbp51* KO)
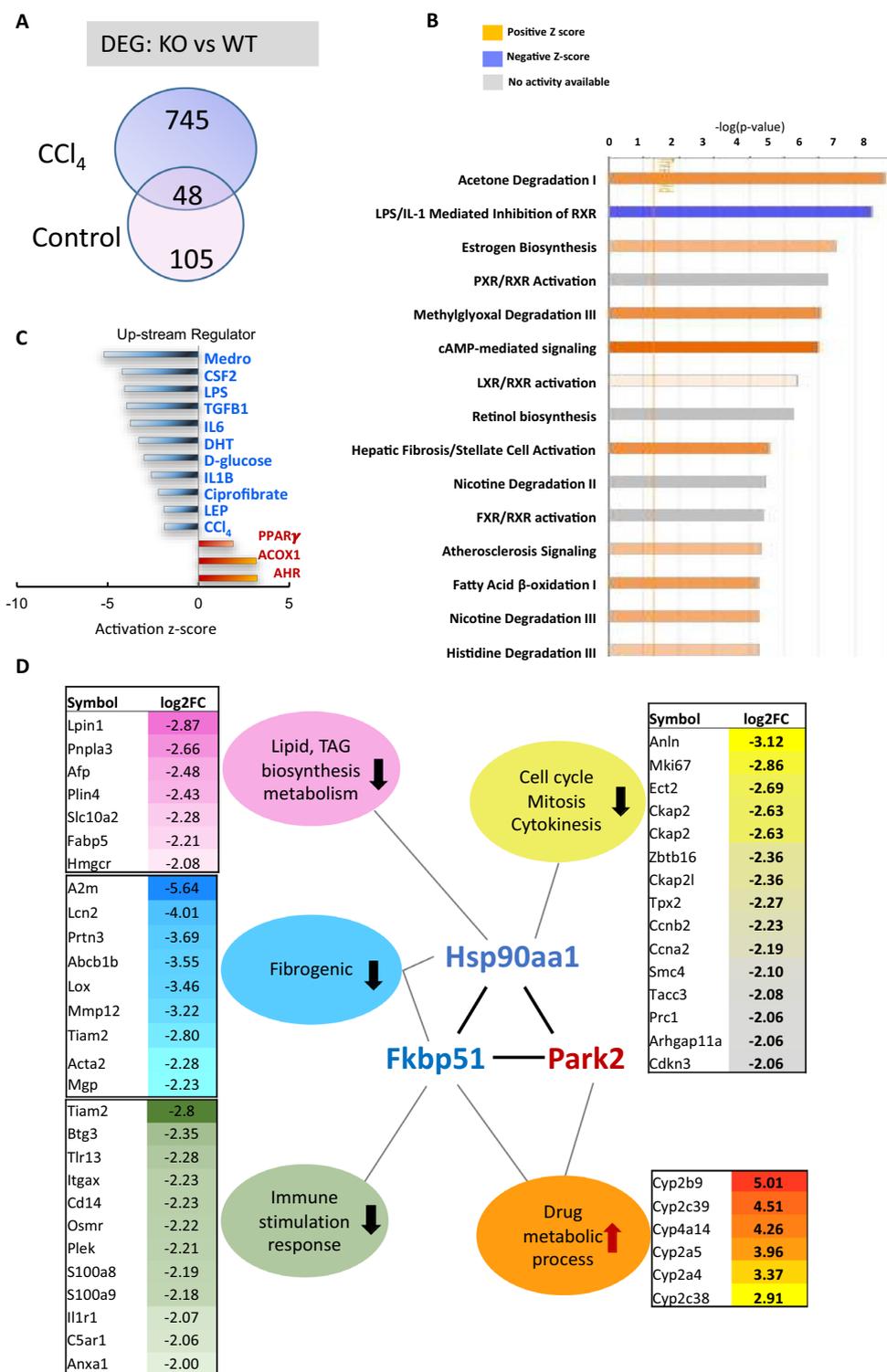
Fig. 2 (See legend on previous page.)

(DHT), and leptin (LEP)], D-glucose, and CCl$_4$ were inactivated, while PPARγ, acyl-coA oxidase 1 (ACOX1), and aryl hydrocarbon receptor (AHR) were activated in KO mice after CCl$_4$ injury, suggesting that FKBP51 plays a role in hormone nuclear translocation, metabolism of glucose, and other functions in response to CCl$_4$-induced

Qiu *et al. Cell & Bioscience*   (2024) 14:1

Page 7 of 25

Table 1 KEGG pathway analysis has identified significant pathways that are different between KO and WT after CCl$_4$-induced liver injury

Pathway description	Observed gene count	FDR	Matching proteins in the data
PPAR signaling pathway	9	7.56E-06	ACSL3,ACSL4,APOA2,APOA5,CYP7A1,CYP8B1,FABP4,FABP5,LPL
Metabolic pathways	27	0.00416	ACSL3,ACSL4,AGXT2L1,ALAS1,ALDH3A2,AMDHD1,ATP6V0C,B3GALT1,CSAD,CYP2E1,CYP7A1,CYP8B1,GCLC,GLUL,HAL,HMGCR,HSD3B2,HSD3B7,HYI,ISYNA1,LPIN1,LPIN2,MOCS1,OAT,RRM2,SPHK2,SQLE
Protein processing in endoplasmic reticulum	9	0.00416	DNAJC3,HSP90AA1,HSP90B1,HSPA5,HYOU1,PDIA3,PDIA4,SSR3,SYVN1
Bile secretion	6	0.00453	ABCG5,ABCG8,CYP7A1,HMGCR,NR0B2,SLC10A2
Amoebiasis	7	0.00506	CD14,COL1A1,COL1A2,COL3A1,COL4A1,COL5A3,IL1R1
ECM-receptor interaction	6	0.00897	COL1A1,COL1A2,COL3A1,COL4A1,COL5A3,SPP1
Protein digestion and absorption	6	0.00897	COL1A1,COL1A2,COL3A1,COL4A1,COL5A3,SLC3A1
Platelet activation	7	0.0104	COL1A1,COL1A2,COL3A1,COL5A3,FGA,FGB,FGG
Primary bile acid biosynthesis	3	0.0181	CYP7A1,CYP8B1,HSD3B7
PI3K-Akt signaling pathway	11	0.0181	CDKN1A,COL1A1,COL1A2,COL3A1,COL4A1,COL5A3,HSP90AA1,HSP90B1,IL6R,NR4A1,SPP1
Glutathione metabolism	4	0.0355	GCLC,GSTA2,GSTM4,RRM2
Transcriptional mis-regulation in cancer	7	0.0355	CD14,CDKN1A,CEBPA,CEBPE,ID2,TMPRSS2,ZBTB16
Glycerolipid metabolism	4	0.047	ALDH3A2,LPIN1,LPIN2,LPL

Table 2 Identified disease and function categories and involved regulators when comparing *Fkbp51* KO and WT after CCl$_4$-induced liver injury

Top regulator effect networks		
Regulators	Disease and function	Consistency score
Akt, APOE, C5, CSF1, CSF2, Ige, IL1, IL17A, IL1A, IL2, KIT	Engulfment of myeloid cells	43.7
Alpha catenin, AR, CSF2, EGFR, FOXA1, GLIS2, IL17A, IL2	Endocytosis, Engulfment of cells	21.1
ACOX1, CREBBP, CSF2, IFI16, IL17A, IL2, OSM, PRKCA, ROCK2	Arteriosclerosis, Endocytosis, Engulfment of cells	12
Akt, Brd4, CSF2, F2, IL17A, KITLG, PRKCD, TLR4	Activation of antigen presenting cells, Endocytosis	20

Table 3 GO analysis predicted functional alterations in *Fkbp51* KO after CCl$_4$-induced liver injury

Function	Category	*p*-value		z-Score
Cellular Movement	Cell movement	3.75E−16	Decreased	−4.673
Cell-To-Cell Signaling and Interaction	Activation of cells	5.45E−10	Decreased	−4.262
Cellular Function and Maintenance, Inflammatory Response	Phagocytosis	2.21E−06	Decreased	−3.891
Inflammatory Response	Immune response of cells	1.28E−07	Decreased	−3.799
Amino Acid Metabolism, Small Molecule Biochemistry	Metabolism of amino acids	4.33E−07	Increased	2.185
Lipid Metabolism, Small Molecule Biochemistry	Conversion of lipid	5.63E−07	Increased	2.312
Organismal Survival	Morbidity or mortality	1.12E−13	Increased	2.442
Organismal Survival	Organismal death	4.81E−13	Increased	2.514

injury (Fig. 2c). It was confirmed that glucocorticoid (GC) and fibroblast growth factor (FGF) levels were lower in KO than WT (S-Fig. 2g, h). Further analysis of downstream effect networks identified the engulfment of myeloid cells, endocytosis, and activation of antigen presenting cells (Table 2). Thus, our data support differential responses between KO and WT mice in the recruitment of myeloid cells to the liver and the secretion

Qiu *et al. Cell & Bioscience*   (2024) 14:1

Page 8 of 25

of inflammatory cytokines through the innate immune system in response to liver injury.

The most significant DEGs with fold changes (FC) > 4 (or Log2 FC > 2) are included in Additional file 1: Table S2, and were further analyzed for their protein–protein interactions using the Search Tool for the Retrieval of Interacting Genes (STRING) database. Five robust functional gene hubs centered by *Hsp90aa1, Fkbp51,* and *Park2* (encodes Parkin) were identified. Genes in each cluster with their gene expression log2FC between KO and WT are listed in Fig. 2d. Prominently, a group of Cyp450 family members were upregulated in KO mice, while DEGs related to cell cycle, lipid biosynthesis, fibrogenesis, and immune-function were down-regulated (Fig. 2d). Further analysis points to FKBP51 as a key player resulting in unique changes in disease and development, physiological systems, signaling pathways, and toxicity following CCl_4 injury (Additional file 2: Fig. S3A). GO analysis predicted functional categories altered in KO after CCl_4 injury (Table 3). Enrichment of biological processes, cellular components, and molecular functions further highlighted functionally-relevant changes between KO and WT mice following liver injury using IPA analysis (Additional file 2: Fig. S3B).

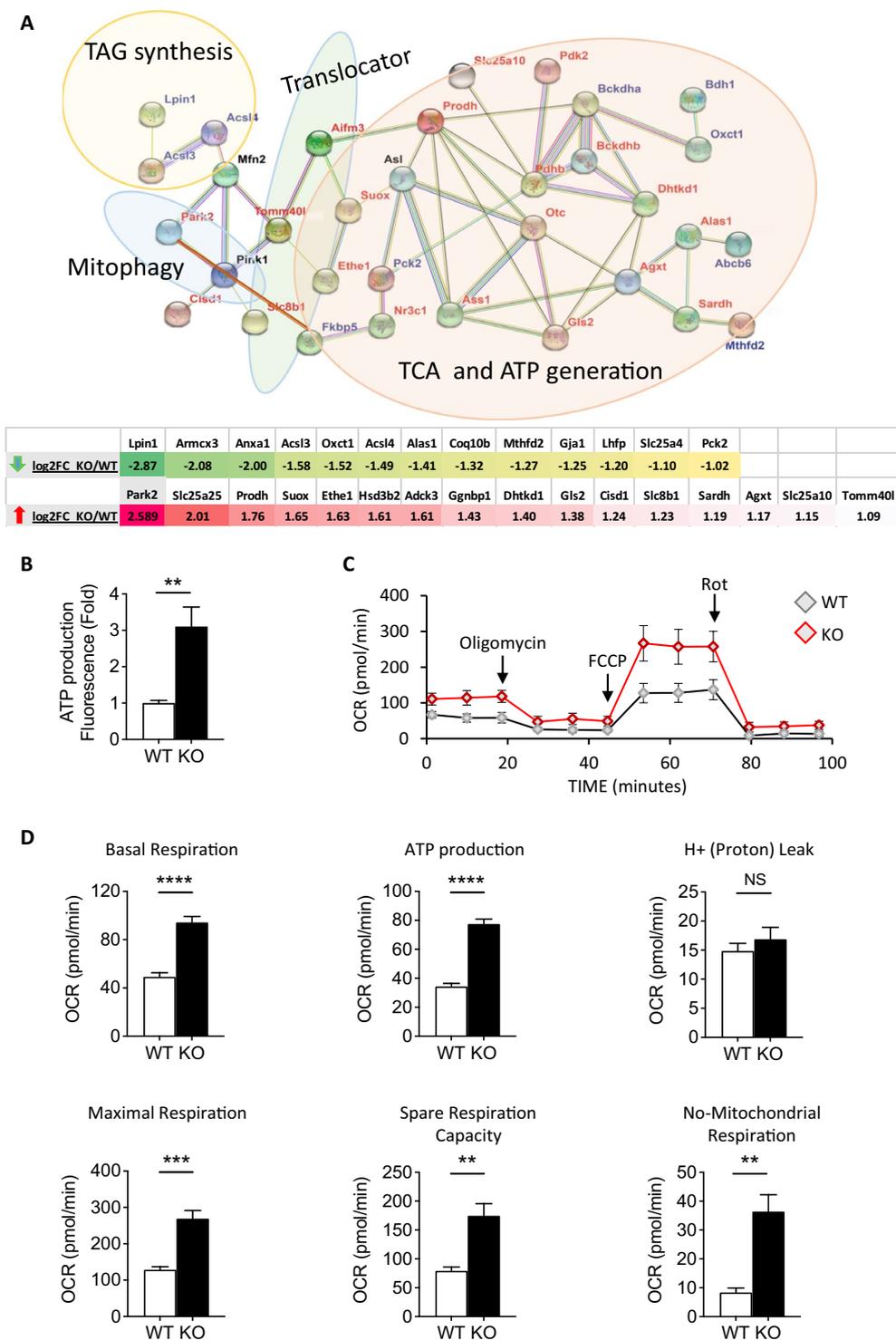### Elimination of *Fkbp51* affects mitochondrial function-related genes and capacity for ATP production

As *Park2* and *Hsp90* are involved in mitochondrial function, we studied DEGs related to mitochondrial function. We observed that DEGs related to mitochondrial function are overrepresented (more than 10%) ($p < 0.05$, FC > 2) in the data set, and the top DEGs were further analyzed (Fig. 3a). STRING analysis was utilized to cluster the genes based on their functional connections. Genes related to triacylglyceride (TAG) synthesis were downregulated (Lipin 1 (*Lpin1*), acyl-CoA synthetase long chain family member 3 (*Acsl3*), and *Acsl4*). Translocator genes [translocase of outer mitochondrial membrane 40 like (*Tomm40l*) and solute carrier family 8 member b1 (*Slc8b1*)], and the mitophagy-related gene Parkin (*Park2*) were upregulated in KO following CCl_4

treatment (Fig. 3a). Additionally, sulfite oxidation-related genes [sulfite oxidase (*Suox*) and ethylmalonic encephalopathy protein 1 (*Ethe1*)] and amino acid degradation-related genes [proline dehydrogenase (*Prodh*), and glutaminase 2 (*Gls2*)] were also upregulated (Fig. 3a). Gene expression fold-changes of these mitochondrial function-related DEGs between KO and WT mice are shown in Fig. 3a. The identification of a functional connection between Parkin and FKBP51 [34], along with the established relationship between Pink1 and FKBP51 [35], strengthens the argument that FKBP51 plays an important role in mitochondrial regulation. Our study further highlights those DEGs with higher FC between KO and WT and their involved functions in mitochondria.

Based on the data demonstrating that mitochondrial function-related DEGs were altered, we compared primary cultured WT and KO mouse embryonic fibroblasts (MEFs) and examined whether they exhibit an intrinsic difference in energy production. Indeed, KO MEFs possess a significant increase in ATP production compared to WT (Fig. 3b). The Seahorse XF Cell Mito Stress Test was conducted to assess mitochondrial respiration differences between cultured KO and WT MEFs, as such differences could affect ATP production. Following sequential treatments of oligomycin, carbonyl cyanide 4-(trifluoromethoxy) phenylhydrazone (FCCP), rotenone (Rot), and antimycin A, the oxygen consumption rate (OCR) was measured at four parameters of mitochondrial function: basal respiration, ATP turnover, proton leak, and spare respiratory capacity (Fig. 3c). The parameter calculations from the above measurements demonstrated that basal respiration, ATP production, maximal respiration, spare respiratory capacity, and non-mitochondrial respiration, were all increased in KO MEFs, while H^+ (proton) leak did not significantly differ between WT and KO MEFs (Fig. 3d). Together, these findings suggest that the loss of *Fkbp51* induces higher mitochondrial function in energy metabolism as measured by ATP production.

(See figure on next page.)

Fig. 3 Loss of Fkbp51 increases ATP production by enhanced mitochondrial function. **A** DEG between *Fkbp51* KO and WT after CCl_4 treatment functionally-related to mitochondria are interconnected based on STRING analysis. Figure was modified from STRING analysis, red-colored gene names indicate upregulation in KO, blue-colored gene names indicate downregulation in KO, and black-colored gene names indicate similar expression between KO and WT (added to identify more interactions). Log2 fold-change (FC) of DEG are included. **B** ATP production of WT and KO MEF cells as determined by PhosphoWork Luminometric ATP Assay. **C** Mitochondrial respiration reflected by OCR was detected in *Fkbp51* KO and WT MEFs during the course of the Seahorse XF Cell Stress Test. The arrow indicates the sequential addition of oligomycin, FCCP, and rotenone (Rot). The OCR profile is normalized to total cultured cell protein. **D** Graph demonstrating increases in KO MEF OCR during basal mitochondrial respiration, ATP production, H^+ (Proton) leak, maximal respiration, spare respiration capacity, and non-mitochondrial respiration relative to WT. Graphs represent mean values ± SEM from 3 independent experiments. *p* values were determined by student's unpaired *t*-test with the statistical significance labeled as follows: ** as $p < 0.01$; *** as $p < 0.001$ and **** as $p < 0.0001$; NS, not statistically significant. Key: WT, wild type; KO, *Fkbp51* KO

A

	Lpin1	Armcx3	Anxa1	Acsl3	Oxct1	Acsl4	Alas1	Coq10b	Mthfd2	Gja1	Lhfp	Slc25a4	Pck2			
⬇ log2FC_KO/WT	-2.87	-2.08	-2.00	-1.58	-1.52	-1.49	-1.41	-1.32	-1.27	-1.25	-1.20	-1.10	-1.02			
	Park2	Slc25a25	Prodh	Suox	Ethe1	Hsd3b2	Adck3	Ggnbp1	Dhtkd1	Gls2	Cisd1	Slc8b1	Sardh	Agxt	Slc25a10	Tomm40l
⬆ log2FC_KO/WT	2.589	2.01	1.76	1.65	1.63	1.61	1.61	1.43	1.40	1.38	1.24	1.23	1.19	1.17	1.15	1.09

B

C

D

Fig. 3 (See legend on previous page.)

Co-localization of Parkin with FKBP51 protein in mitochondria

Our above RNA-seq data indicate that *Fkbp51* KO possess upregulated *Park2* expression (Fig. 3a), a gene crucial for mitochondrial function and cytoskeleton formation [36–39]. We confirmed a higher *Park2* mRNA expression in KO mice compared to WT by real-time PCR (Fig. 4a). While CCl_4 treatment decreased the mRNA expression

in both groups, *Park2* was still higher in KO mice compared to WT (Fig. 4a). Based on these findings, Parkin protein expression in KO was studied using IHC and western blotting. Liver IHC revealed that Parkin expression is increased in KO mice when compared to WT, regardless of CCl_4 treatment (Fig. 4b, c). Western blotting confirmed that Parkin protein levels are higher in KO mice versus WT both at baseline and following CCl_4 treatment (Fig. 4d). Moreover, Parkin protein expression is higher in both the enriched mitochondrial fraction and cytosolic fraction in KO mice (Fig. 4e–h). We previously found that Parkin posttranslational modification (PTM) is regulated by FKBP51 protein in hippocampus, with no difference in *Park2* mRNA, but significantly higher Parkin expression in KO relative to WT [34]. Consistently, higher protein expression of Parkin was observed in KO livers as compared to WT under both control and CCl_4 treatment. However, CCl_4 treatment decreased the Parkin mRNA in WT and KO suggesting differences between tissue and treatment effects.

To understand these differences at the cellular level, mitochondria (MitoTracker labeling) and Parkin were tracked in WT and KO MEF cells. Parkin was expressed strongly in the cytoskeleton, more densely in KO MEFs than WT MEFs, particularly in the perinuclear area (Fig. 4i). A robust increase in mitochondrial network signal intensity of Parkin was observed in KO (Fig. 4i, magnified panel) and confirmed by Manders' overlap coefficient score (Additional file 2: Fig. S4A), a result consistent with findings in western blotting (Fig. 4e, f). *Fkbp51* KO demonstrates a significant increase in Parkin expression (Fig. 4i and quantification in Additional file 2: Fig. S4B) and Parkin plays a critical role in mitochondrial function. This is in agreement with previously published co-immunoprecipitation (Co-IP) results demonstrating an interaction between Parkin and FKBP51 proteins [34]. Further identification of the co-localization of Parkin and FKBP51 could be an indication of their functional interaction within the cell. The HepG2 liver cell line was used for co-transfection experiments. Flag-*FKBP5*1 was transfected into HepG2 cells and was detected using an anti-Flag antibody. As shown in Fig. 4j, reduced expression of Parkin was observed due to higher FKBP51 expression, thus Flag-Fkbp51 and Parkin merged images show only weak Parkin labeling, a result consistent with our previously published mechanism. Overexpression of FKBP51 via Flag-Fkbp51 plasmid transfection led to a significant and dose-dependent decrease in endogenous Parkin expression (Fig. 4j) [34]. The Manders' overlap coefficient score in Additional file 2: Fig. S4C demonstrates that FKBP51 is co-localized with Parkin. Additionally, in HepG2 cells, FKBP51 and Parkin were found to co-localize within mitochondria networks, with more intense labeling observed in the perinuclear area (Fig. 4j, middle and right, and Additional file 2: Fig. S4C). The co-localization of FKBP51 and Parkin in the mitochondria could partially explain how *Fkbp51* affects mitochondrial function, serving as a Parkin regulator.

Ablation of FKBP51 increases mitochondrial size and induces autophagy/mitophagy in the liver

To evaluate how the loss of FKBP51 affects mitochondrial function and Parkin-associated MQC at the subcellular level, mitochondrial morphology was assessed by electron microscopy (EM) [40]. Interestingly, KO liver cells were initially observed to possess larger mitochondria compared to WT mouse livers both at baseline and after CCl_4 treatment (Fig. 5a). The quantification of randomly selected microphotographs, measuring 250–300 mitochondria, demonstrated that the KO exhibited significantly larger mitochondria than the WT, regardless of whether they were under control conditions or CCl_4 treatment (Fig. 5b). Additionally, it was observed that CCl_4 treatment had no impact on the size of mitochondria for either genotype, as compared to the control treatment (Fig. 5b). However, no difference in mitochondria number was observed between KO and WT in either condition (Fig. 5c).

(See figure on next page.)

Fig. 4 *Fkbp51* KO mice have a higher expression of Parkin than WT. **A** Quantitative PCR analyses reveal that *Fkbp51* KO liver expresses more *Park2* mRNA relative to WT in both control and CCl_4-treated conditions. **B** Immunohistochemical labeling demonstrates an increase in Parkin in KO, and a CCl_4–associated increase in both WT and KO. **C** Quantitation of AOD of Parkin in liver sections. **D** Western blotting confirms a higher level of Parkin in control (Con) KO liver, with an apparent increase of Parkin in WT following CCl_4 treatment. **E**–**H** Increased Parkin expression in total KO liver lysates as well as in enriched mitochondrial and cytoplasmic fractions as compared to WT. Graphs represent mean values ± SEM from 6 mice for each group. *p* values were determined by student's unpaired *t*-test (**F**–**H**) or two-way ANOVA (**A**, **C**, **D**) with the statistical significance labeled as follows: *as $p < 0.05$, **as $p < 0.01$, *** as $p < 0.001$ and **** as $p < 0.0001$. **I** A comparison of *Fkbp51* KO and WT MEFs confirms that the absence of FKBP51 is associated with higher levels of Parkin, more intense MitoTracker signal, and localization to the mitochondria. Magnified images outlined by the yellow boxes in the merged images are presented on right. Immunofluorescent labeling of Parkin and MitoTracker showed higher intensity of Parkin signal in KO than WT MEF cells, particularly in the perinuclear area and along the mitochondrial network. **J** Immunofluorescent labeling reveals the co-localization of FKBP51 and Parkin with mitochondria in HepG2 cells transfected with Flag-*Fkbp51*. Key: WT, wild type; KO, *Fkbp51* KO; AOD, average optical density; Con, control; Mito, mitochondria

Qiu *et al. Cell & Bioscience*   (2024) 14:1

Page 11 of 25
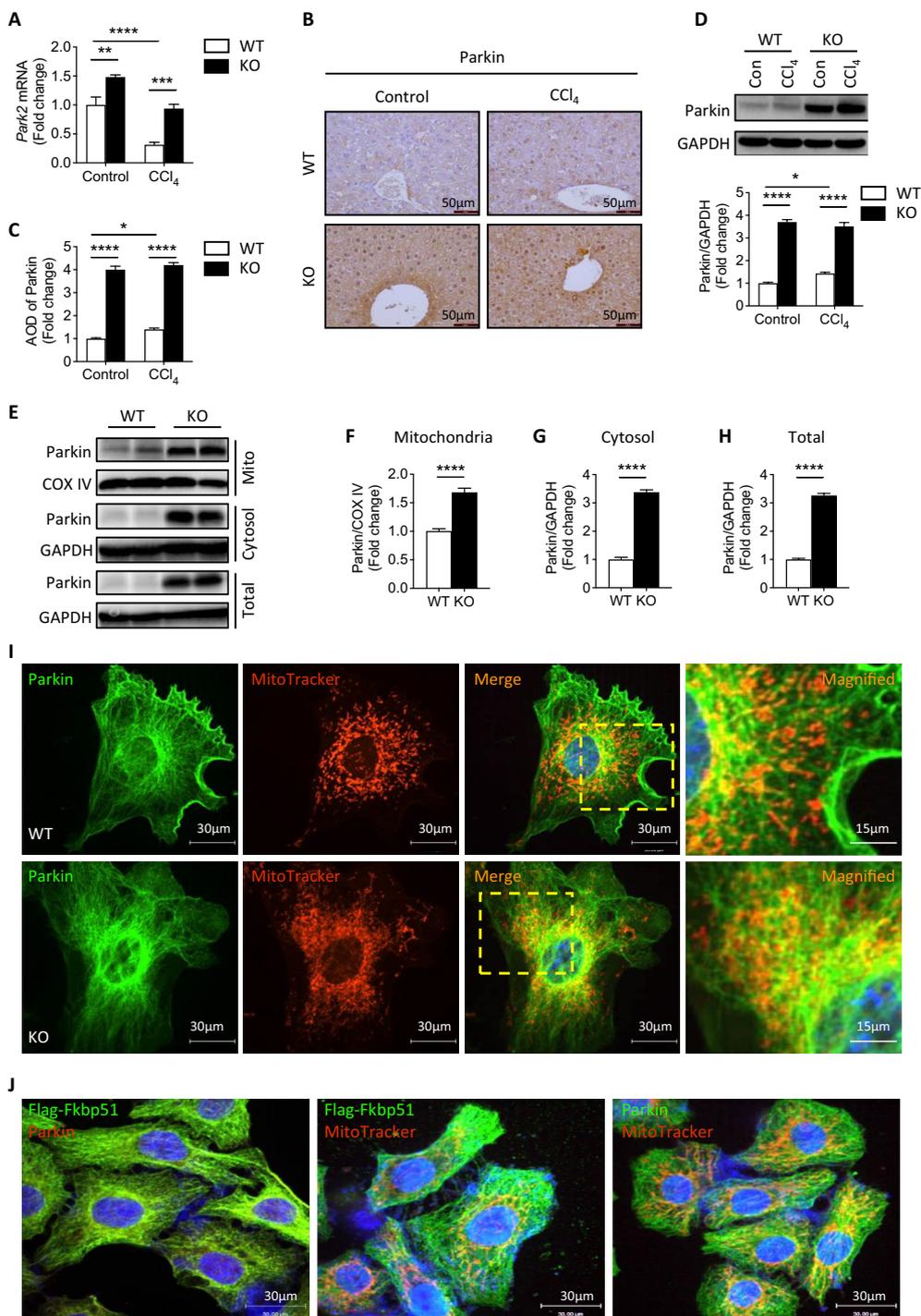
Fig. 4 (See legend on previous page.)

No obvious ER morphological difference was observed between KO and WT in control treatment (Fig. 5d). After CCl$_4$ treatment however, we observed more mitochondrial damage and ER expansion (arrowhead), with wrinkled and broken mitochondrial membranes (Fig. 6a–c), in WT mice, while the ER appeared normal in KO (Figs. 5d KO panel, 6d, e) with occasional ER expansion (Fig. 6f). The formation of mitochondrial-derived vesicles (MDVs) serves as a defense mechanism to remove harmful mitochondrial components and as a mechanism of immune

Qiu *et al. Cell & Bioscience*   (2024) 14:1

Page 12 of 25
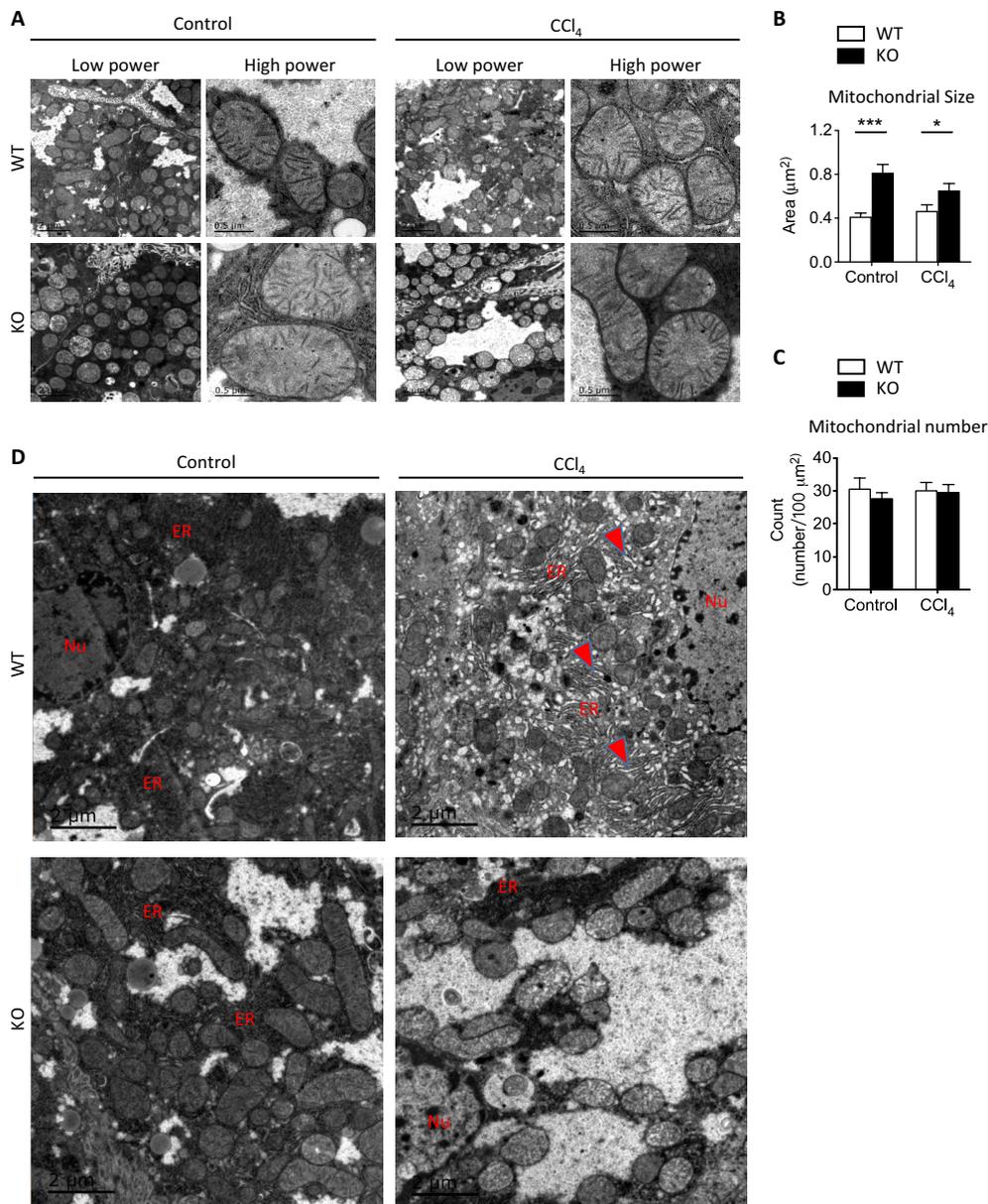
Fig. 5 Liver mitochondria are larger in *Fkbp51* KO mice than in WT. **A** Representative EM photomicrographs of WT and KO liver mitochondria with or without CCl_4 treatment. **B**, **C** Mitochondrial size (area) quantification demonstrated that *Fkbp51* KO mitochondria are larger in both control and CCl_4 conditions, although no differences in mitochondrial number were detected. Quantifications are from random representative microphotographs measuring 250–300 mitochondria. *p* values were determined by two-way ANOVA with the statistical significance labeled as follows: *as $p < 0.05$, *** as $p < 0.001$. **D** Representative EM photomicrographs depict ER expansion in WT following CCl_4 treatment. Key: WT, wild type; KO, *Fkbp51* KO; Nu, nucleus; ER, endoplasmic reticulum

tolerance and immune response. MDVs were observed in both but more often in KO compared to WT mice after CCl_4 treatment (Fig. 6c in WT vs. Figure 6e, f, k in KO). Laminated bodies (LB) and MDVs to be released to the lysosome (L) were identified more prominently in KO mice (Fig. 6d, f, g, h, i, l). Remarkably, more occurrences of mitophagy (Fig. 6j, k, red arrows) were observed in

KO mice versus WT after CCl_4 treatment. The lighter appearance of some KO mitochondria was observed following CCl_4 treatment, which may relate to its unique adaptation to insult (Fig. 5d and Additional file 2: Fig. S5). These EM images provided morphological evidence that KO mitochondria were better protected from CCl_4 injury in than WT. To further identify molecular evidence to
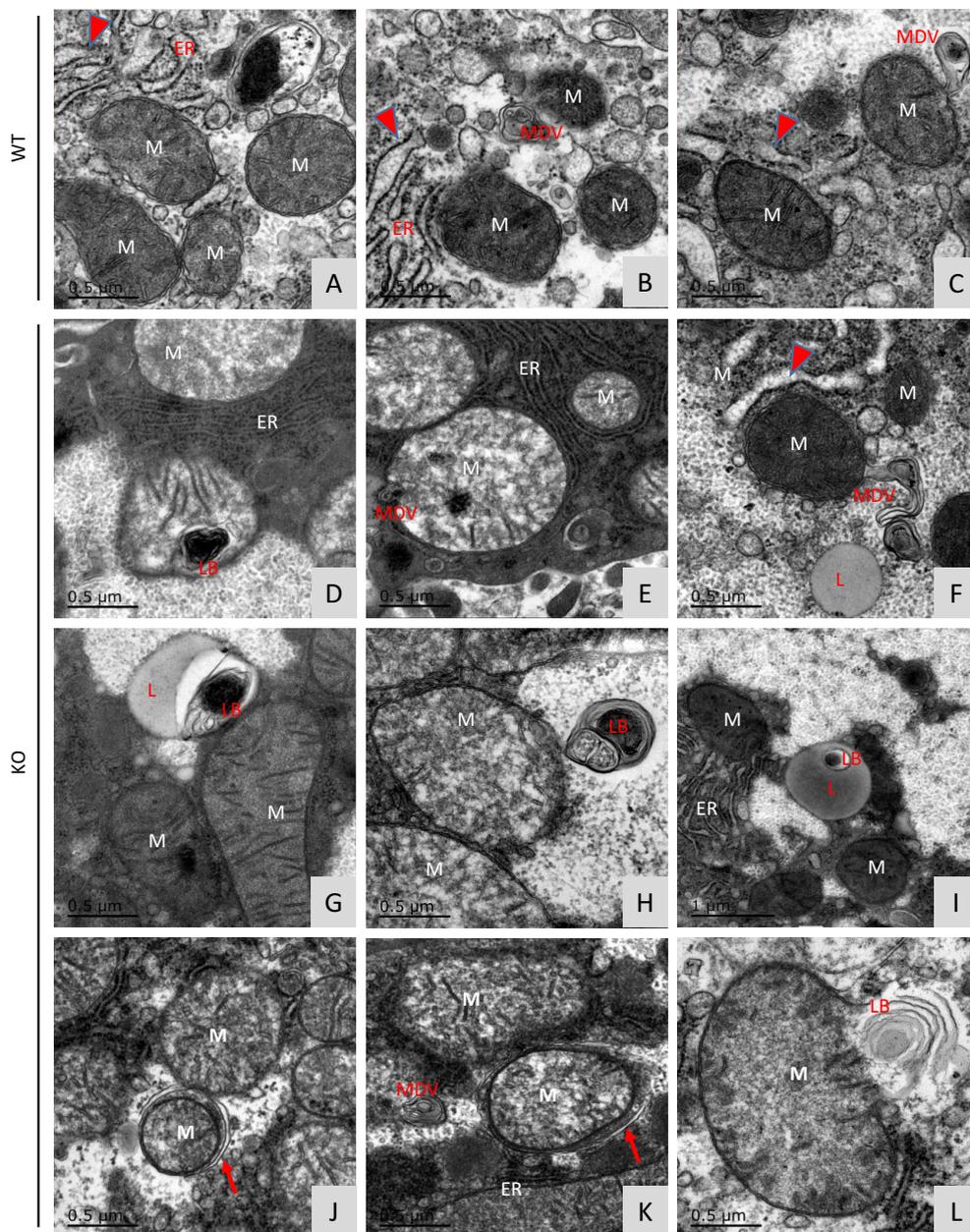
Fig. 6 Representative EM images reveal more MDVs and mitophagy in *Fkbp51* KO liver after CCl₄ injury. **A** ER expansion (red arrow) and **B** damaged mitochondria with incomplete membranes were observed more often in WT. Mitochondrial derived vesicles (MDV) were found in both WT (**B**, **C**) and KO (**E**, **F**, **K**), but more occurrence was found in KO. **D** Normal ER in KO with laminated bodies (LB) formed inside mitochondria. **E** Normal ER and dense particles observed inside mitochondria with multiple MDVs inside and at border of mitochondria. **F** Lysosome close to MDVs, and ER expansion (arrow) was occasionally observed around damaged mitochondria in KO. **G** Lysosome with a dense laminated body. **H** Laminated bodies with damaged granule bodies. **I** LB within lysosome with. **J**, **K** More mitophagy was observed in KO and representative mitophagosomes are indicated by the red arrows. **L** Mitochondria, ER, and LB in close contact during clearance of mitochondrial debris. Key: WT, wild type; KO, *Fkbp51* KO; ER, endoplasmic reticulum; M, mitochondria; MDV, mitochondrial derived vesicles; LB, laminated bodies; L, lysosome

support these observations, protein-related to mitochondrial damage clearance (mitophagy) and MDV processes were studied.

Mitophagy is an autophagy process for the removal of damaged mitochondria and is regulated by several important proteins including Parkin, dynamin-related protein 1 (DRP1), ubiquitin-binding protein p62 (also
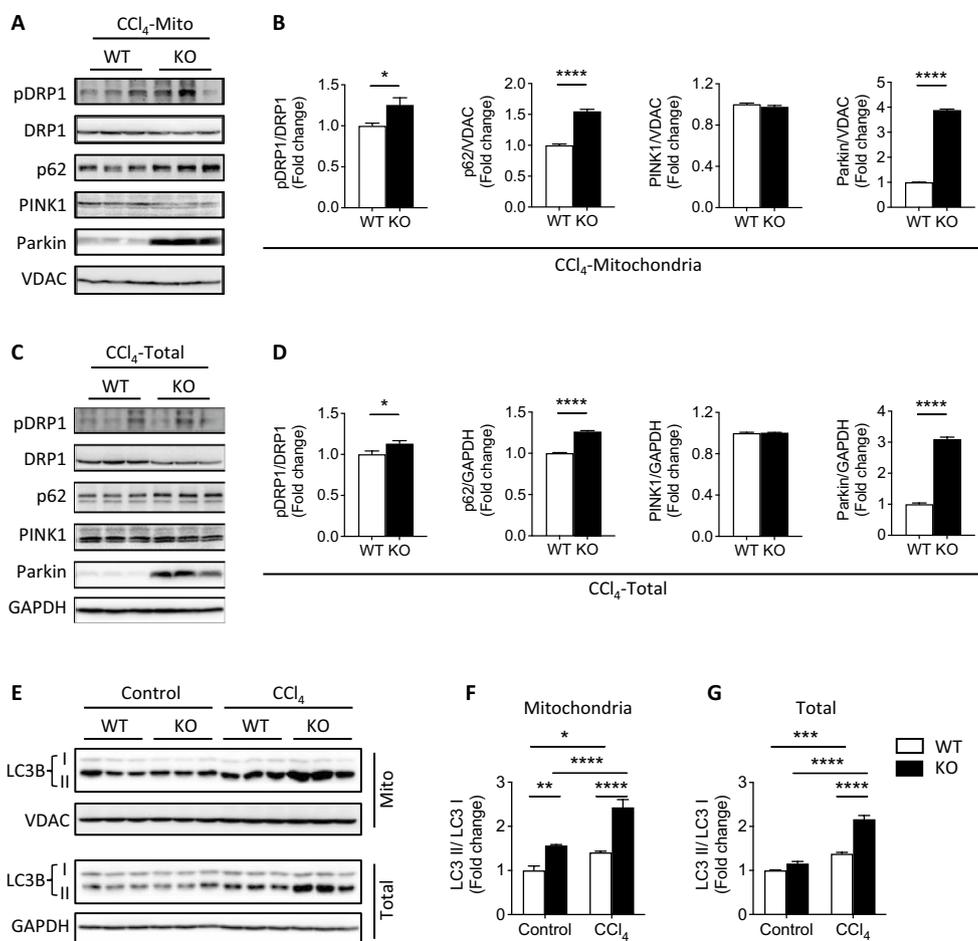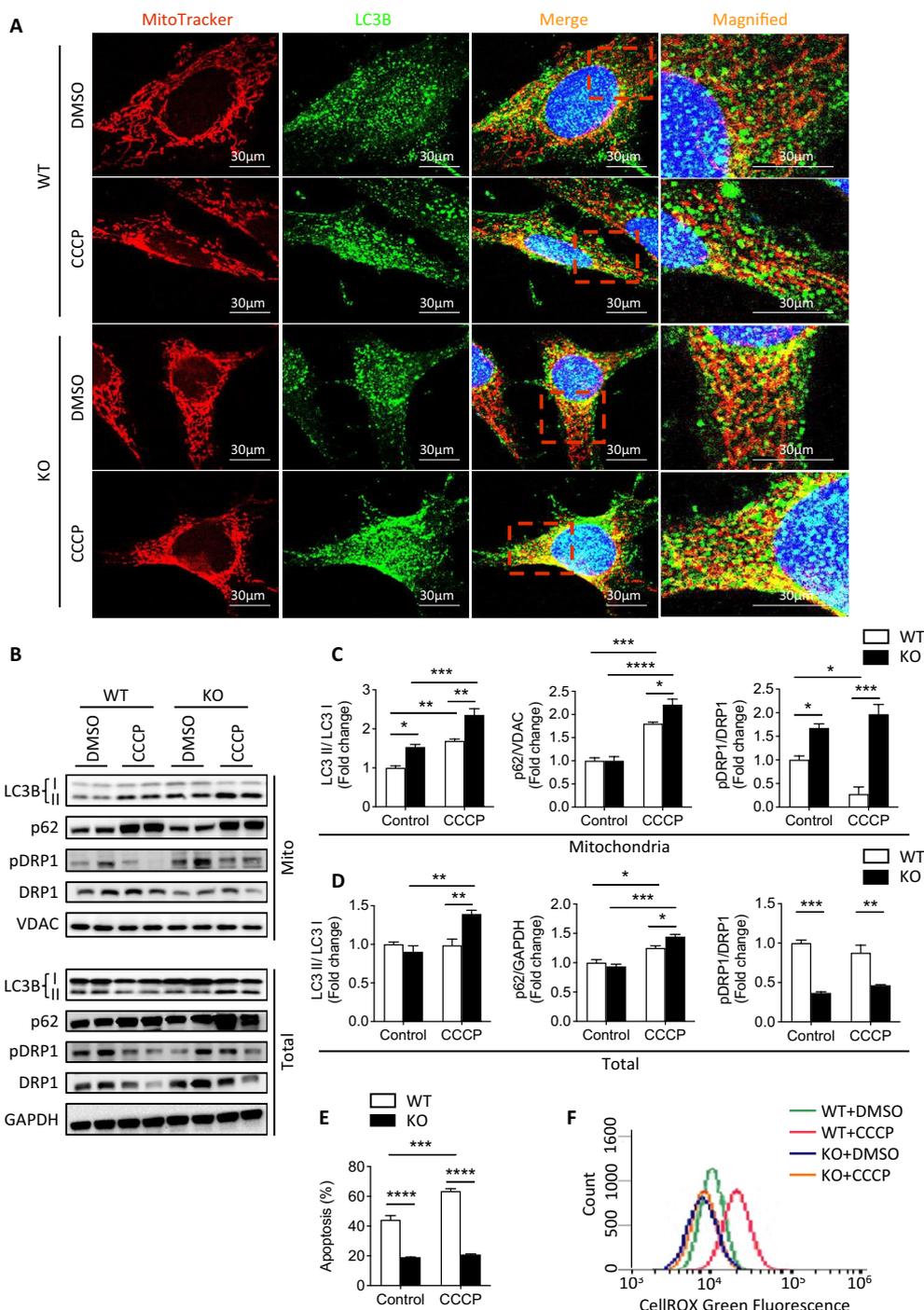
Fig. 7 Increased autophagy/mitophagy in *Fkbp51* KO livers. **A**, **C** Immunoblots depict mitochondrial and total p-DRP1, DRP1, p62, PINK1, Parkin, and respective loading controls in CCl$_4$-treated liver. **B**, **D** Densitometry ratios of target proteins relative to loading control in the mitochondrial and total fractions from **A** and **C**, respectively. **E–G** Immunoblots depict mitochondrial and total LC3B and respective loading controls in livers. Densitometry revealed higher LC3B II/I ratios in KO of mitochondria fraction and total protein following CCl$_4$ treatment. Graphs represent mean values ± SEM from 6 mice for each group. *p* values were determined by student's unpaired *t*-test for (**B**, **D**) or two-way ANOVA for (**F**, **G**) with the statistical significance labeled as follows: *as $p < 0.05$, **as $p < 0.01$, *** as $p < 0.001$ and **** as $p < 0.0001$. Key: WT, wild type; KO, *Fkbp51* KO; Mito, mitochondria

known as Sequestosome 1, an autophagy receptor), and PINK1 [41–43]. Consistent with results shown above (Fig. 4f–h), a significant increase of Parkin expression was found in the mitochondrial and total protein fractions of KO mice relative to WT after CCl$_4$ injury. Relative to WT, KO exhibited higher p-DRP1/DRP1 ratios in both mitochondrial and total protein fractions, as well as increased p62 expression, but no change in PINK1 expression after CCl$_4$ injury (Fig. 7a–d). Initialization of the mitophagosome requires microtubule-associated protein light chain 3B (LC3B) to degrade damaged mitochondria [44]. LC3B protein was measured in livers from untreated and CCl$_4$-treated

WT and KO mice. The ratio of LC3B II/I significantly increased after CCl$_4$ treatment, particularly in KO mice, indicating increased autophagosome activity (Fig. 7e–g). The in vivo and in vitro data support a critical role for FKBP51 affecting mitochondrial dynamics, including increased occurrences of mitophagy and MDVs and less ER swelling in KO mice. Enhanced autophagy/mitophagy may explain the amelioration of CCl$_4$-induced liver injury in the KO liver [40].

Fkbp51 KO MEF cells demonstrate increased autophagy/mitophagy marker expression and reduced ROS after CCCP treatment

To directly test whether FKBP51 plays a role in mitophagy, proton ionophore carbonyl cyanide

Fig. 8 Treatment with CCCP enhances autophagy/mitophagy, particularly in *Fkbp51* KO. **A** *Fkbp51* KO and WT MEFs treated with DMSO or CCCP were assessed for the expression of the autophagy/mitophagy marker LC3. Both *Fkbp51* KO and WT exhibit increased expression of LC3, localizing to the mitochondria, with *Fkbp51* KO expressing the highest in both conditions. **B**–**D** Western blotting revealed KO exhibiting higher levels of LC3B II/I and p62/VDAC in mitochondrial and total fractions following CCCP treatment. Levels of pDRP1/DRP1 were higher in KO mitochondria, but lower in the total fraction. **E** Evaluation of apoptosis in control and CCCP treatment. **F** ROS levels were assessed by CellROX Green fluorescence intensity via flow cytometry. CCCP treatment showed a peak shift in WT MEFs only. Graphs represent mean values ± SEM from 3 independent experiments. *p* values were determined by two-way ANOVA with the statistical significance labeled as follows: *as $p < 0.05$, **as $p < 0.01$, *** as $p < 0.001$ and **** as $p < 0.0001$. Key: WT, wild type; KO, *Fkbp51* KO; Mito, mitochondria

m-chlorophenylhydrazone (CCCP), a mitochondrial uncoupler, was used to induce mitochondrial damage in primary cultured MEFs, and LC3B and p62, pDRP1, DRP1 were measured to assess mitochondrial stress [45]. Consistent with previous results, KO cells showed enhanced MitoTracker signal compared to WT, with decreased labeling intensity under CCCP treatment

(Fig. 8a and quantification in Additional file 2: Fig. S6A). LC3B signals of both WT and KO MEFs were enhanced following CCCP treatment, with greater labeling intensity observed in KO MEFs (Fig. 8a and quantification in Additional file 2: Fig. S6B). Merged images of MitoTracker and LC3B indicate greater mitophagy in KO MEFs, as signified by a stronger yellow signal
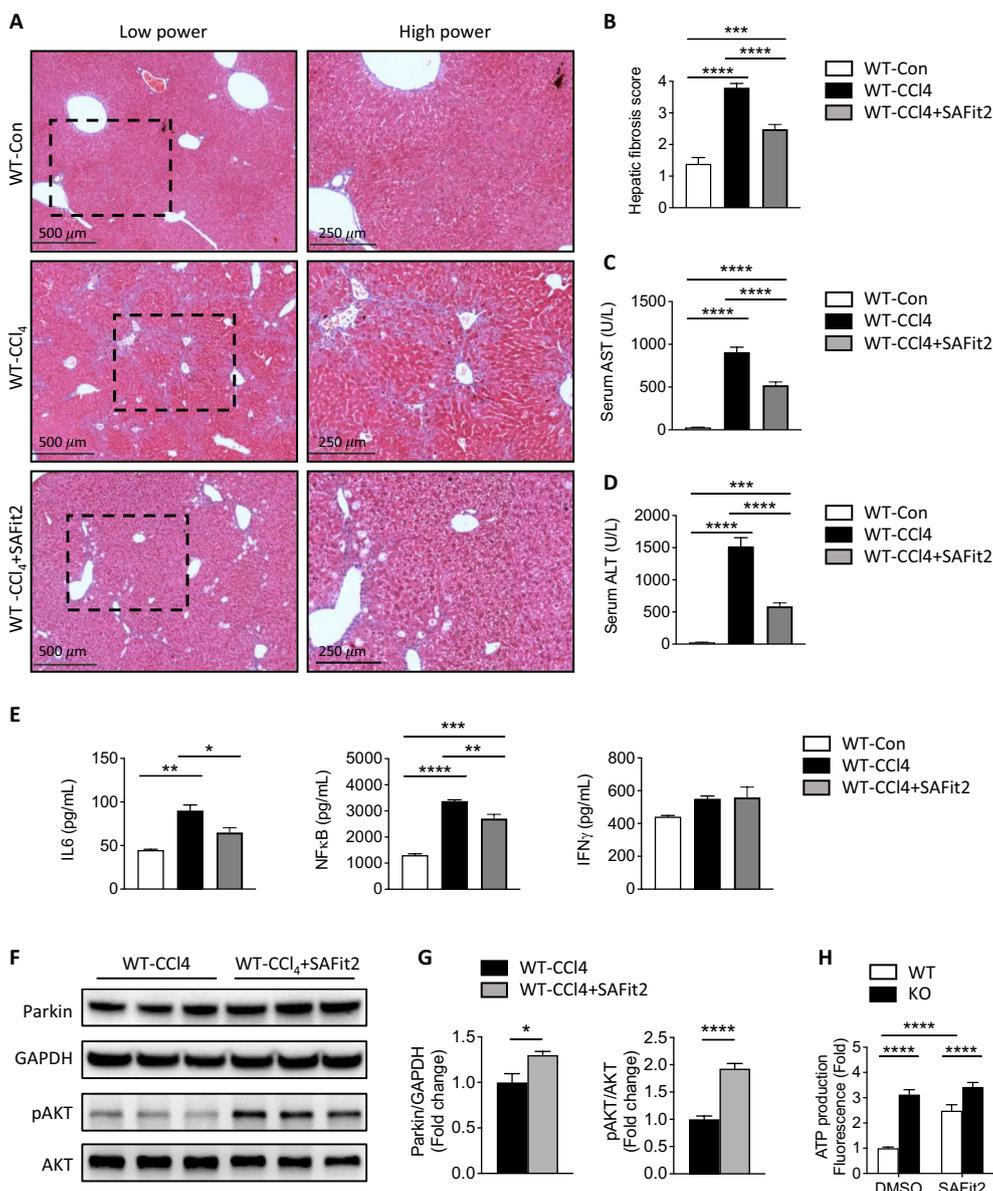
Fig. 9 FKBP51 inhibitor SAFit2 attenuates CCl4-induced liver fibrosis and injury. **A** Masson's trichrome staining of livers after treatment with SAFit2 in CCl4-induced liver fibrosis. **B** Assessment of liver fibrosis score. **C**, **D** AST and ALT levels are reduced with SAFit2. **E** SAFit2 application reduced serum IL6 and NFκB, but no effect on IFN-γ level. **F**, **G** Western blotting revealed an increase in Parkin and pAKT expression in WT-CCl4 treated with SAFit2 mice. Graphs represent mean values ± SEM from 5–6 mice for each group. **H** Normalized ATP production from WT and KO MEF cells treated with SAFit2. Graph represents mean values ± SEM from 3 independent experiments. *p* values were determined by student's unpaired *t*-test (**F**), one-way ANOVA (**B**–**E**) or two-way ANOVA (**H**) with the statistical significance labeled as follows: *as $p < 0.05$, **as $p < 0.01$, *** as $p < 0.001$ and **** as $p < 0.0001$. Key: WT, wild type; KO, *Fkbp51* KO

(Fig. 8a) and Manders' overlap coefficient score (Additional file 2: Fig. S6C). Western blotting data support that the ratio of LC3B II/I is significantly higher in KO MEFs compared to WT after DMSO control treatment in the mitochondrial fraction and after CCCP treatment in both the mitochondrial and total protein fractions (Fig. 8b–d). Following CCCP treatment, p62 was increased in both fractions of KO and WT MEFs, though it was significantly higher in KO than in WT (Fig. 8b–d). Additionally, the mitochondrial p-DRP1/DRP1 ratio was higher in KO MEFs than WT before and after CCCP treatment but the total protein p-DRP1/DRP1 ratio was lower in KO than WT, suggesting that KO MEFs are more protected from CCCP-induced shifts in mitochondrial dynamics (Fig. 8b–d). The above data support an enhancement of autophagy/mitophagy function in *Fkbp51* KO MEF cells, protective mechanisms for preventing mitochondrial damage.

Although we demonstrated that more apoptotic cells are present in CCl_4-treated WT liver than in KO (Fig. 1i, j), a direct difference of apoptosis was assessed resulting from mitochondrial damage induced by CCCP. In addition to confirming the presence of fewer apoptotic cells in KO, a significant increase of apoptosis was found in WT cells after CCCP treatment (Fig. 8e). Additionally, a CCCP-induced increase in the level of ROS was detected solely in primary cultured WT MEFs as indicated by peak shifting (Fig. 8f). This provided indirect evidence that KO cells produce fewer ROS during mitochondrial insult, which could partially explain the protective effect observed in KO mice following CCl_4 treatment. Thus, these data support better MQC in *Fkbp51* KO through the regulation of mitophagy/autophagy processes, mitochondrial morphology and dynamics, and ATP production.

Inhibition of FKBP51 with SAFit2 increases Parkin and ameliorates CCl_4-induced liver injury

We applied a highly specific selective FKBP51 inhibitor (SAFit2) to test its efficacy in preventing liver injury. SAFit2 has previously been applied in other studies and no toxicity was demonstrated with long-term treatment [46–48]. Concurrent injection of CCl_4 and SAFit2 reduced indicators of liver injury, including lower intensity of trichrome staining (Fig. 9a) and lower quantified hepatic fibrosis scores (Fig. 9b). Serum AST and ALT levels were reduced in CCl_4+SAFit2-treated WT mice (Fig. 9c, d). Additionally, inhibition of SAFit2 led to a decrease in the levels of IL-6 and NFκB in the serum (Fig. 9e), which is in line with the observation that KO mice exhibit lower levels of IL-6 and NFκB (Additional file 2: Fig. S2). However, the inhibition by SAFit2 shows a lesser effect on IFN-γ (Fig. 9e). Consistent with the results from *Fkbp51* KO, SAFit2 inhibition was associated with a commensurate increase in Parkin (Fig. 9f, g). FKBP51 is a chaperone to AKT-specific phosphatase. Previously, elevated AKT phosphorylation was observed in Fkbp51 KO cells and SAFit2 inhibition of FKBP51 increased pAKT2 [11, 14]. To confirm the SAFit2 inhibition effect, pAKT and AKT were measured after SAFit2 application, and the increased ratio of pAKT/AKT suggested a consistent functional regulatory outcome (Fig. 9f, g). We further studied mitochondrial functional alterations after FKBP51 inhibition by measuring ATP production in vitro. WT and KO MEFs were treated with SAFit2, and ATP production was increased specifically in WT MEFs (Fig. 9h). The data support that inhibition of FKBP51 by SAFit2 prevents CCl_4-induced liver injury, potentially via regulation of ATP production in the mitochondria.

Discussion

In this study, we demonstrated that loss of FKBP51 function ameliorates liver injury partially via enhanced mitochondrial quality control. *Fkbp51* KO mice exhibited enhanced mitochondrial function (ATP production) and better protection of cellular function through mitochondrial protection (MDVs and mitophagy) after CCl_4 injury. RNA-seq analysis pointed out multiple pathways and genes associated with this protective effect. Mitochondrial function-associated genes were enriched and we found that Parkin is significantly upregulated in KO in both basal and CCl_4-treated conditions in addition to other genes with high-fold change and significant *p*-value. STRING analysis identified inter-connections between *Fkbp51*, *Hsp90aa1*, and *Park2*, and a hub of genes related to lipid and TAG biosynthesis and metabolism, fibrogenesis, immune response, cell cycle, and drug metabolism. We have previously demonstrated the interaction of FKBP51 and Parkin using immunofluorescence (IF) and co-immunoprecipitation [34]. In the current study, we found that these two proteins co-localize in mitochondria. Treatment with the selective FKBP51 inhibitor SAFit2 also substantiated its effectiveness as a means of reducing liver injury, confirming FKBP51 to be a useful therapeutic target. Together, these findings support the conclusion that targeting FKBP51 represents a novel mechanism to protect against liver injury.

Previously, we demonstrated the prevention of HFD-induced fatty liver and alcohol-induced liver injury using our *Fkbp51* KO model [13, 18]. In our current study, the first line of evidence includes the results from the histological and biochemical analyses and the observed downregulation of multiple genes that are functionally related to fibrogenesis in KO. For example, downregulation of the α-2 macroglobulin (*A2m*) gene and TIMP1 protein

were found in *Fkbp51* KO following CCl$_4$ treatment. In human research, the serum levels of these two markers are reliable predictors of NASH and alcoholic liver disease risks [50]. Secondly, genes involved in increasing TAG degradation and reducing TAG biosynthesis were found in *Fkbp51* KO mice. The downregulation of Patatin-like phospholipase domain-containing protein 3 (*Pnpla3*) in KO mice is consistent with human research, where genetic variants of *PNPLA3* have been linked to non-alcoholic steatohepatitis (NASH) and NAFLD [51], and higher liver TAG content [52]. Increased levels of the NAFLD-linked PNPLA3 isoform result in larger lipid droplets, while decreasing PNPLA3 results in an opposite trend [53]. Thus, lower expression of *Pnpla3* in *Fkbp51* KO suggests the potential for less lipid deposition, consistent with reduced TAG biosynthesis and enhanced lipid metabolism. Previous studies using our *Fkbp51* KO highlight the importance of FKBP51 in GR and PPARγ function, potentially through the regulation of the AKT and p38 pathways [13, 14]. In WT mice, activation of PPARγ results in elevated PPARγ-induced genes, such as lipoprotein lipase (LPL), which is moderately lower in *Fkbp51* KO [13–15]. In our study, we found the PPAR signaling pathway to be significantly altered in CCl$_4$-treated KO and WT (Table 1). Upstream regulator effects analysis predicted PPARγ activation in KO after CCl$_4$ liver injury (Fig. 2c). However, the activation of PPARγ resulted in upregulation of LPL to a much higher degree in WT (8x) than KO (2x). Activation of GR and PPARγ in this model needs to be investigated further. Interestingly, the expression of genes involved in fatty acid biosynthesis were downregulated in *Fkbp51* KO after CCl$_4$ injury, including *Lpin1*, *Acsl3*, and *Acsl4*. Mice lacking *Lpin1* demonstrate faster recovery from endotoxin administration and enhanced autophagic clearance; results consistent with the protection from liver injury observed in *Fkbp51* KO mice [54]. Additionally, we found increased expression of CYP450 member genes including Cyp2A5 and Cyp2c39. Cyp2A5 protects against ALD development and drug-induced liver injury [55, 56], and upregulation of Cyp2c39 expression may reduce liver retinoic acid accumulation and liver fibrosis due to its function in retinoic acid catabolism [57]. Pathway and function analysis pointed out that inflammation, mitochondria, and oxidative metabolism are physiological systems likely involved in the protection of liver injury in *Fkbp51* KO mice. Thus, multiple lines of evidence from gene expression, biomedical function, and physiological alterations in the *Fkbp51* KO are consistent with human findings.

FKBP51 was first identified as a GR binding protein, negatively regulating GR activity, but further studies revealed its role in post-translational protein modification (PTM) [5, 58]. Consistently, *Fkpb51* elimination enhances GR inhibition and lowers glucocorticoid expression in serum. Previous research found that FKBP51 directly regulates AKT phosphorylation and participates in autophagy processes [59] and other protein PTM [60–62]. In our study, FKBP51 inhibition by SAFit2 results in up-regulation of pAKT, which is consistent with previous observations of their relationship. Recently, we have found that FKBP51 directly binds to Parkin and affects its PTM [34]. Our data suggests the potential involvement of FKBP51 in the autophagy/mitophagy process via upregulation of Parkin, as Parkin is known to play a critical role in mitophagy [63, 64]. As an important regulator of mitophagy and mitochondrial function, Parkin protects against alcohol-induced liver injury and steatosis [39]. Additional studies of Parkin-associated mitochondrial proteins determined that acyl-CoA synthetase long-chain family members ACSL1 and ACSL4 are involved in mitochondrial metabolism [65]. Interestingly, we found that *Acsl3* and *Acsl4* are downregulated in *Fkbp51* KO and that they share a gene hub with *Park2*. Parkin is a known critical member of MQC processes, including mitophagy and MDVs, and we propose that FKBP51 participates in these processes through the regulation of Parkin activity, as evidenced by the increased number of MDVs observed in KO. Thus, regulation of Parkin and mitochondrial quality control by FKBP51 represents a promising avenue for disease treatment, and could also enhance related functions including the degradation of misfolded proteins, autophagy/mitophagy, and MDVs [66, 67].

FKBP51 is a co-chaperone of HSP90 and functions as an isomerase, which is critical for protein folding and binding. This data set also suggested protein binding activity to be the most significant altered molecular function. By inhibiting mitochondria-localized members of the HSP90 family, cytosolic HSP90 was shown to be required for the proper folding of PINK1 [68]. Mitochondrial HSP90 is needed for protein import and the assembly of a multiprotein complex activating PINK1- and Parkin-dependent MQC. It is also possible that FKBP51/HSP90 plays a cochaperone function in the folding and disaggregation of proteins in mitochondrial compartments and participates in this MQC. Consistently, *Hsp90aa1* gene expression is found to be downregulated in *Fkbp51* KO following liver injury. RNA-seq data suggests that mitochondrial function associated genes are enriched, and the noted increase in ATP production and reduction in ROS production after liver injury indicate enhanced mitochondrial function. Increased mitophagy was evidenced by EM and molecular markers. Thus, multiple lines of evidence suggest that *Fkbp51* is a critical gene for mitochondrial

function and quality control via regulation of one or more key components.

CCl4-induced liver injury and fibrosis have resulted in immune response and microphages infiltration (20, 21). In our study, GO analysis predicted the functional including decreased inflammatory response and increased lipid metabolism (Table 3). As an immunophilin protein, FKBP51 functions in immune response and mitochondrial function. It has been demonstrated that FKBP51 shuttling between the mitochondria and the nucleus is involved in the regulation of proinflammatory cytokines, and that its depletion reduces the expression of type I IFN following infection [20]. Furthermore, FKBP51 was demonstrated to play roles in the control of NFκB and TGFβ signaling, whereas the inhibitory immune checkpoint programmed cell death 1 (PD1) and its ligand (PD-L1) promote alternative splicing of the *FKBP51* gene [69]. The silencing of FKBP51 results in reduced cytokine and chemokine secretion [70]. It is likely that the protection conferred to KO mice may be due in part to the minimal increases in some immune factors including TGFβ, NFκB, IL6, and many more after CCl_4 treatment in our study. Pathway analysis in our research has identified that the top regulatory differences in the WT and KO response to CCl_4 injury are the engulfment of myeloid and endocytosis. Myeloid cells play a major role in the sensitization to liver injury, and the myeloid cell-liver axis is critically important in chronic liver disease [71]. Thus, these results have begun to illuminate immune-specific roles of *Fkbp51* in CCl_4-induced liver injury. More specifically, our findings are in line with prior research on these immune function-related genes. The KO mice also downregulated immune-relevant genes, such as lipocalin 2 (*Lcn2*), which is critical in innate immunity. Previous studies found that *Lcn2* KO mice have enhanced mitochondrial function and differential redistribution of linoleic acid in the inner mitochondrial membrane [72], and *Lcn2* is critical for cell proliferation, autophagy, and mitochondrial biogenesis and liver function [73, 74]. Other immune function-related genes are also worth mention here, such as CD14, Il1r1, and Tiam2 are downregulated in KO after CCl_4 injury. CD14 is a surface antigen and mediates innate immune response, CD14 controls Toll-like 4 endocytosis and is implicated in liver disease [75–78]. T-lymphoma invasion and metastasis-inducing protein 2 (Tiam2) is required for signal transduction pathways involved in the regulation of cytokinesis and implicated in liver physiology and cancer development were found down regulated in *Fkbp51* KO [79, 80]. The function of FKBP51 in regulating the immune response to liver injury remains a question warranting further investigation.

One limitation of this research is that the in vitro molecular analyses use MEF cells and hepatocytes. In the future, genetic modification of *Fkpb51* in specific liver cell types should be considered to understand the role of *Fkbp51* in fibrosis. Macrophages and Kupffer cells should be considered first due to their high expression of *FKBP51* in humans (https://www.proteinatlas.org/ENSG00000096060-FKBP5). It is important to note that the induction levels of IL-6 and NFκB in response to CCl_4 treatment in WT mice (Fig. 9e) appear to be inconsistent with the results depicted in Additional file 2: Fig. S2, which show no significant change in WT mice with and without CCl_4. We have identified two notable factors that may contribute to these variations. Firstly, there is a difference in the injection schedule (Additional file 2: Fig. S7), and secondly, DMSO was used as a solvent control in Fig. 9e (further details in the Additional file 2: Fig. S7 and method section). It is possible that the results can be explained by the fact that DMSO can modulate the activity of NKT and NK cells [49].

In summary, our study highlighted the impact of *Fkbp51* in multiple pathways and genes that are associated with better endo-phenotypes (liver enzymes, histology, pro-inflammatory factors) in *Fkbp51* KO mice after CCl_4-induced liver injury. Knockout of *Fkbp51* protects against CCl_4-induced liver injury via the promotion of MQC (including the enhancement of mitochondrial respiration, reduced oxidative stress, and apoptosis), downregulation of some immune response-related genes, increased expression of some Cyp450 family members, and increased mitophagy. Additionally, the downregulation of cell cycle-associated genes after liver injury in *Fkbp51* KO echoes its function in cell proliferation and cancer [81–84]. FKBP51 regulation of Parkin activity in the liver is a novel mechanism to explore for future treatments making the inhibition of FKBP51 a promising strategy in the treatment of liver injury.

Materials and methods
Animals
All experimental protocols were approved by the Animal Care and Research Advisory Committee of the Institute of Laboratory Animal Science, Chinese Academy of Medical Sciences & Peking Union Medical College, Beijing. The animals were maintained in facilities fully accredited by the Association for the Assessment and Accreditation of Laboratory Animal Care (AAALAC). Development of *Fkbp51* KO mice was described in a previous publication [85]. *Fkbp51* KO and WT littermates were bred through heterozygous (*Fkbp51*±) mating. Only male mice were used in this study. WT mice weigh approximately 25 g at 8 weeks of age, while KO weigh approximately 23 g.

Mouse model of liver fibrosis

Male 8-week-old WT and *Fkbp51* KO mice were randomly assigned into either olive oil injection control or CCl$_4$ injection treatment groups. Modified protocol was followed from previous publication [35, 86]; specifically, mice were injected intraperitoneally (IP) three times weekly for 2 weeks with olive oil (vehicle, sigma-aldrich, MO, USA) or carbon tetrachloride (CCl$_4$, sigma-aldrich, MO, USA) diluted 1:9 in olive oil at a dose of 5 µl/g of body weight (BW). A schematic diagram illustrating the injection procedure can be found in Additional file 2: Fig. S7a. Mice were sacrificed 48 h after the final injection, and their livers were harvested after being perfused with ice-cold saline, except in the case of Fig. 1a. For Fig. 1a, the purpose was to compare and analyze the overall liver phenotype among the groups, including evaluating the original color displayed by each group.

Histological analysis and measurements of serum cytokines

Paraffin embedded liver sections at 4 µm thickness were prepared for Masson's trichrome, immunohistochemistry (IHC), and TUNEL labeling. Masson's trichrome staining was performed following the manufacturer's instructions (Abcam, MA, USA) and photomicrographs were acquired using a CTR6000 microscope with a DFC450 C camera (Leica, Wetzlar, Germany). The hepatic fibrosis score was evaluated from eight randomly selected fields, as described [32]. IHC was performed as previously described [34]. A list of antibodies used in this study is included in Additional file 1: Table S3. DAB-based TUNEL assay kit (#ab206386, Abcam, MA, USA) was used to measure apoptosis in the liver according to the manufacturer's instructions. After mice were anesthetized by 0.02 g/ml tribromoethanol (18 µl/g BW), blood was collected from the abdominal aorta using coagulation tubes (BD, NJ, USA). Supernatants were collected for the measurement of cytokines with ELISA detection kits according to the manufacturer's instructions. A list of ELISA kits used in this study is included in Additional file 1: Table S4.

RNA-seq data analysis

RNA-seq expression profiling was performed on vehicle control- and CCl$_4$-treated KO (n=3) and WT (n=3) mice (n=12 total). Liver tissues were snap frozen and RNA was isolated using TRIzol® followed by RNeasy Mini kit purification (Qiagen, Hilden, Germany). Sequencing and data analysis were performed as previously published [87], with the exception that the reads were aligned to the reference *Mus musculus* genome (UCSC build MM9) with TopHat [88]. DEGs were identified between KO and WT at different *p*-value cut offs.

Multiple test adjustments were also performed to control for false positives with an adjusted (adj) *p*-value of < 0.05 using the Benjamini–Hochberg adjustment [89] and sequence read abundances with readCount > 50 or rpkm > 1. The significant genes with Fold Change (FC) > 2 were analyzed further. Heatmaps of gene expression levels were generated with R/heatmap2. Genes that were differentially expressed between KO and WT following treatment were analyzed using IPA, Ingenuity®, and GO enrichment analysis.

Cellular ATP, metabolism assays, and immunocytochemistry (ICC)

Primary WT and *Fkbp51* KO MEFs were cultured and passaged as previously described [85]. Cellular ATP synthesis in WT and KO MEFs was determined by PhosphoWork Luminometric ATP Assay Kit (AAT Bioquest, Inc, CA, USA) according to the manufacturer's protocol. The cells were lysed in 100 µl ATP assay solution and the luminescence intensity was recorded on a luminometer (Thermo Fisher Scientific, MA, USA). ATP production was normalized to protein concentration measured by the BCA method. Mitochondrial function was evaluated by XF Cell Mito Stress Test using the XF24 Extracellular Flux Analyzer (Seahorse Bioscience, MA, USA) according to the manufacturer's instruction. Briefly, cells were seeded in the XF24 cell culture microplate at 1×10^4 cells/well the day before testing. Cells were washed and cultured in pre-warmed assay medium (XF Base Medium contained with 5 g/L glucose, 2 mM pyruvate, 2 mM L-glutamine, pH 7.4) and placed in an incubator without CO$_2$ for 1 h prior to the assay. After measurement of baseline oxygen consumption rate (OCR), the hydrated sensor cartridges were loaded with oligomycin (1 µM), FCCP (1 µM), and rotenone (0.5 µM) to measure ATP-related OCR, maximal respiration-related OCR and non-mitochondrial respiration-related OCR, respectively. The data were calculated with the XF Stress Test Report Generator according to the user guide and normalized to protein concentration. To induce mitophagy, primary WT and KO MEFs were treated with CCCP (Sigma-Aldrich, MO, USA) at a final concentration of 10 µM for 18 h. HepG2 cells were cultured in Dulbecco's Modified Eagle Medium (DMEM, Gibco, NY, USA) containing 10% fetal bovine serum (Gibco) and penicillin (Gibco). The cells were transfected with Flag-*Fkbp51* (HG11487-CF, Sino Biological, Beijing, China) using lipofectamine 3000 (Thermo Fisher Scientific, MA, USA) according to the manufacturer's recommendations. MitoTracker Red (Thermo Fisher Scientific, MA, USA) was used to identify mitochondria according to manufacturer's instruction. Briefly, after indicated treatment, the cells were incubated with MitoTracker at a final concentration of 200 nM at 37°C

Qiu *et al. Cell & Bioscience*   (2024) 14:1

Page 21 of 25

for 30 min. After being washed with warmed DMEM and PBS, the cells were fixed with 4% paraformaldehyde, and ICC was performed using anti-FKBP51, anti-Parkin, or anti-LC3 antibodies as previously described [34]. The fluorescence signal was captured using confocal laser scanning microscopy (Leica TCS LSI, Germany). A list of antibodies used in this study is included in Additional file 1: Table S3. The quantitative colocalization was performed using Manders' overlap coefficient determined by Fiji ImageJ software with the BIOP Jacop plugin [90]. This coefficient will vary from 0 to 1, the former corresponding to non-overlapping images and the latter reflecting 100% co-localization between both images. The relative normalized mean fluorescence intensity (MFI) of target protein per cell was quantified using ImageJ.

Isolation of mitochondria from liver and MEF cells

Either 200 mg minced liver tissue or 10^6 MEF cells were homogenized with 1 ml isolation separating medium (containing 5 mM HEPES, 220 mM mannitol, 70 mM sucrose, 1 mM PMSF, 0.2% BSA, and 1 µg/ml aprotinin, pH 7.4) as described [91]. After centrifuging at $1,000 \times g$ for 10 min at 4 ℃, the supernatants were collected and centrifuged at $10,000 \times g$ for 10 min at 4 ℃. The cytoplasmic fraction in supernatants were collected and the mitochondria in pellets were resuspended with 5 volumes of reserve medium (separating medium without BSA and aprotinin). The protein concentrations were determined using the Pierce BCA kit (Thermo Fisher Scientific, IL, USA).

Western blotting and quantitative real-time PCR (qPCR)

Proteins from liver were harvested in lysis buffer with 1:10 volume of protease inhibitor and 1:100 volume of phosphatase inhibitor cocktail (Roche, IN, USA) as previously described. Western blotting was performed as previously described [92–94]. The primary antibodies used in this research include anti-COX IV, -DRP, -p-DRP, -FKBP51, -GAPDH, -LC3B, -P62, -Parkin, -Pink1, and -VDAC. Detailed information for these antibodies and vendors is listed in Additional file 1: Table S3. Signals were captured and quantified using the Chemiluminescent Imaging System. Liver mRNA was isolated using TRIzol® (N=3–5). Reverse transcription (RT) and qPCR were conducted according to the manufacturer's instructions (TaKaRa Biotechnology, Dalian, China) using the ABI PRISM 7500 System (Thermo Fisher Scientific, MA, USA). The relative mRNA expression levels were normalized to *Gapdh*, which was not differentially expressed between KO and WT groups. Primer sequences are listed in Additional file 1: Table S5.

Transmission electron microscopy (EM)

Mouse liver tissues were cut into approximately 1 mm cubes, fixed in 2.5% Glutaraldehyde in 0.1 M Phosphate Buffer (pH 7.4), and post-fixed in 1% osmium tetroxide. The samples were then rinsed with sodium cacodylate buffer and dehydrated with gradient alcohol, replaced by propylene oxide and embedded in Epon 812 (Sigma-Aldrich). Semi-thin Sects. (1 µm) were cut, stained by methylene blue, and oriented under a light microscope. Ultra-thin sections were stained with uranyl acetate and lead citrate and were monitored under a JEM-1400 electron microscope (JEOL, Tokyo, Japan). The mitochondrial size from around 200 fields for each group were measured by Fiji *Image J* software.

Cellular apoptosis and reactive oxygen species (ROS) analysis

Primary WT and KO MEFs were cultured with or without CCCP (10 µM) for 18 h. Apoptotic cells were detected using 10 µl/ml Annexin V (BioVision, CA, USA). Data were acquired with a BD FACS Canto II flow cytometer and analyzed with FlowJo (Treestar, OR, USA). For ROS measurement, the cells were treated with CellROX Green (Thermo Fisher Scientific, MA, USA) at a final concentration of 5 µM and incubated at 37 ℃ for 30 min. After washing three times with warmed PBS, the cells were collected, and the ROS level was determined by flow cytometry (BD Biosciences, CA, USA). The fluorescence intensity was determined from 10,000 cells per sample. The data were analyzed using BD Csampler Software and displayed in Histogram (BD Biosciences, CA, USA).

In vivo and in vitro SAFit2 treatment

Male WT mice were randomly assigned to one of three groups (i) Control injection, (ii) CCl_4 injection, or (iii) SAFit2 concurrent with CCl_4 injection (n=5–6 mice/group). CCl_4 was delivered at the same dosage as the earlier experiment three times a week for 2 weeks. The stock solution of SAFit2 (10 mM in 623 µl DMSO) was diluted in 0.9% NaCl to achieve a final volume of 12 ml, resulting in a DMSO concentration of 5% v/v. The SAFit2 was administered via intraperitoneal injection on the day following the CCl_4 injection, with a dosage of 12 µl/g of body weight. The final dosage of SAFit2 was 6 mg/kg of body weight per day; a dose that has been used in other studies and is well tolerated over a prolonged period of time [11, 95]. As a control for SAFit2, an equal concentration of DMSO (5% v/v) dissolved in saline was injected. A schematic diagram illustrating the injection procedure can be found in Additional file 2: Fig. S7B. Liver and blood were collected for liver histology, protein assays, and serum AST and ALT measurement. MEFs from KO

and WT were treated with SAFit2 at 30 μM for 12 h and ATP levels were measured.

Statistical analysis

All values are presented as mean ± standard error of the mean (SEM). Comparisons between two groups were performed using Student's *t*-test, while comparisons for multiple group differences were performed using one-way analysis of variance (ANOVA) or two-way ANOVA, followed by a Student-Newman–Keuls test. GraphPad Prism was used for data analysis (GraphPad Software Inc.), and significance was defined as $p < 0.05$.

Abbreviations

ACOX1	Acyl-CoA oxidase 1
Acsl3	Acyl-CoA synthetase long chain family member 3
AHR	Aryl hydrocarbon receptor
AKT/PKB	AKR mouse strain that develops spontaneous thymic lymphomas/protein kinase B
ALD	Alcoholic liver disease
ALT	Alanine aminotransferase
AST	Aspartate transaminase
ATP	Adenosine triphosphate
CCCP	Carbonyl cyanide m-chlorophenylhydrazone
CCl$_4$	Carbon tetrachloride
COXIV	Cytochrome C oxidase IV
CTGF	Connective tissue growth factor
DEG	Differentially expressed genes
DHT	Dihydrotestosterone
DRP1	Dynamin-related protein 1
EM	Electron photomicrographs
ER	Endoplasmic reticulum
Ethe1	Ethylmalonic encephalopathy protein 1
FCCP	Carbonyl cyanide 4-(trifluoromethoxy) phenylhydrazone
FGF	Fibroblast growth factor
FKBP51	FK506 binding protein 51
GC	Glucocorticoid
Gls2	Glutaminase 2
GR	Glucocorticoid receptor
HCC	Hepatocellular carcinoma
HPA axis	Hypothalamus–pituitary–adrenal axis
HSC	Hepatic stellate cell
HSP90	Heat-shot protein 90
ICC	Immunocytochemistry
IF	Immunofluorescence
IFN-γ	Interferon-γ
IHC	Immunohistochemistry
IL1	Interleukin-1
IP injection	Intraperitoneal injection
IPA	Ingenuity pathway analysis
KEGG	Kyoto encyclopedia of genes and genomes
KO	Knockout
LC3B	Microtubule-associated protein light chain 3B
Lcn2	Lipocalin-2
LEP	Leptin
Lipin1	Lipin 1
LPS	Lipopolysaccharides
LXR	Liver X receptor
MDVs	Mitochondrial-derived vesicles
MEF	Mouse embryonic fibroblast
MQC	Mitochondrial quality control
NAFLD	Non-alcoholic fatty liver disease
NASH	Non-alcoholic steatohepatitis
NFκB	Nuclear factor-κB
OCR	Oxygen consumption rate
p62/SQSTM1	Ubiquitin-binding protein P62/sequestosome 1
PD-1/PD-L1	Programmed cell death 1 and its ligand
PINK1	PTEN Induced Kinase 1
Pnpla3	Patatin-like phospholipase domain-containing protein 3
PPARγ	Peroxisome proliferator-activated receptor gamma
Prodh	Proline dehydrogenase
PTM	Post-translational protein modification
ROS	Reactive oxygen species
RXR	Retinoid X receptor
SAFit2	A selective inhibitor of FKBP51
SEM	Standard error of the mean
Slc8b1	Solute carrier family 8 member b1
STRING	Search Tool for the Retrieval of Interacting Genes
Suox	Sulfite oxidase
TAG	Triacylglyceride
TGF-β1	Transforming growth factor-β1
TIMP1	Tissue inhibitor of metalloproteinase 1
TNF-α	Tumor necrosis factor-α
Tomm40l	Translocase of outer mitochondrial membrane 40 like
TUNEL staining	Terminal deoxynucleotidyl transferase deoxyuridine triphosphate nick end staining
WT	Wildtype
α-SMA	Alpha smooth muscle actin

Supplementary Information

The online version contains supplementary material available at https://doi.org/10.1186/s13578-023-01184-3.

> **Additional file 1. Table S1**: Gene list of IPA Pathway. **Table S2**: DEGs with high fold change. **Table S3**: Antibody list for Western blotting, IHC, and IF. **Table S4**: ELISA kit for serum cytokines analysis. **Table S5**: Primer list for qRT-PCR.
>
> **Additional file 2. Fig. S1**: Immunohistochemical comparisons of Control and CCl4-treated *Fkbp51* KO and WT liver sections. Expression patterns of **A** Collagen I, **B** CTGF, and **C** α-SMA are all higher in the livers of CCl4 treated WT mice than in KO mice. Key: WT, wild type; KO, *Fkbp51* KO. **Fig. S2**: Serum analyses of Control and CCl4-treated *Fkbp51* KO and WT were performed to determine the concentrations of **A** IFN-γ, **B** IL-6, **C** TGF-β1, **D** NFκB, **E** IL-10, **F** TNF-α, **G** GC, and **H** FGF. Graphs represent mean values ± SEM from 6 mice for each group. *p* values were determined by two-way ANOVA with the statistical significance labeled as follows: *as *p* < 0.05, ** as *p* < 0.01 and **** as *p* < 0.0001. Key: WT, wild type; KO, *Fkbp51* KO. **Fig. S3**: **A** IPA pathway analysis identified disease and development, physiological system and development, signaling pathways, and toxicity-related changes as different between KO and WT after CCl4 injury. **B** Go analysis further suggested the enrichment of biological process, cellular component, and molecular function. The top 10 relevant pathways are included in the bar graph. **Fig. S4**: The quantification for Fig. 4i, j. **A** Increased cololization of Parkin/MitoTracker in KO MEFs. **B** The increased relative normalized MFI of Parkin per cell in KO MEFs. **C** Colocalization between Flag-FKBP51/Parkin, Parkin/Flag-FKBP51, Flag-FKBP51/MitoTracker and Parkin/MitoTracker. Graph represents mean values ± SEM from 3 independent experiments. *p* values were determined by student's unpaired *t*-test (**A**, **B**) with the statistical significance labeled as follows: *** as *p* < 0.001, **** as *p* < 0.0001. Key: WT, wild type; KO, *Fkbp51* KO. **Fig. S5**: Representative EM photomicrographs demonstrate that KO has less ER expansion than WT, and KO liver mitochondria are lighter in appearance than WT mitochondria after CCl4 treatment. **Fig. S6**: The quantification for Fig. 8a. **A**, **B** The relative normalized MFI of Mitotracker and LC3B per cell from both genotype under DMSO or CCCP treatment. **C** Colocalization between LC3B/MitoTracker. Graph represents mean values ± SEM from 3 independent experiments. *p* values were determined by two-way ANOVA with the statistical significance labeled as follows: *** as *p* < 0.001, **** as *p* < 0.0001. Key: WT, wild type; KO, *Fkbp51* KO. **Fig. S7**: Schematic diagrams depicting the injection procedures for the animal models.

Qiu *et al. Cell & Bioscience*   (2024) 14:1

Page 23 of 25

Availability of data and materials
The datasets generated during and/or analyzed during the current study are not publicly available due to an additional publication is in preparation using this data set but are available from the corresponding author on reasonable request.

Declarations

Ethics approval and consent to participate
All experimental protocols were approved by the Animal Care and Research Advisory Committee of the Institute of Laboratory Animal Science, Chinese Academy of Medical Sciences & Peking Union Medical College, Beijing. The animals were maintained in facilities fully accredited by the Association for the Assessment and Accreditation of Laboratory Animal Care (AAALAC).

Consent for publication
Not applicable.

Competing interests
The authors declare that there is no conflict of interest in this paper.

Author details
[1]Department of Medicine, Indiana University, School of Medicine, Indianapolis 46202, USA. [2]Department of Surgery, Indiana University, School of Medicine, Indianapolis 46202, USA. [3]Department of Pediatrics, Indiana University, School of Medicine, Indianapolis 46202, USA. [4]Department of Psychiatry, Indiana University, School of Medicine, Indianapolis 46202, USA. [5]Institute of Laboratory Animal Science, Chinese Academy of Medical Sciences & Peking Union Medical College, Beijing 100021, China. [6]General Surgery Department, Peking University People's Hospital, Beijing 100032, China. [7]Department of Pharmacology, Yale University School of Medicine, New Haven, CI 06520, USA. [8]Greehey Children's Cancer Research Institute, UT Health, San Antonio, TX 78229, USA.

References
1. Friedman SL. Liver fibrosis—from bench to bedside. J Hepatol. 2003;38(Suppl 1):S38-53.
2. Ma X, McKeen T, Zhang J, Ding WX. Role and mechanisms of mitophagy in liver diseases. Cells. 2020. https://doi.org/10.3390/cells9040837.
3. Lee WS, Sokol RJ. Liver disease in mitochondrial disorders. Semin Liver Dis. 2007;27:259–73. https://doi.org/10.1055/s-2007-985071.
4. Mansouri A, Gattolliat CH, Asselah T. Mitochondrial dysfunction and signaling in chronic liver diseases. Gastroenterology. 2018;155:629–47. https://doi.org/10.1053/j.gastro.2018.06.083.
5. Criado-Marrero M, et al. Hsp90 and FKBP51: complex regulators of psychiatric diseases. Philos Trans R Soc Lond B Biol Sci. 2018. https://doi.org/10.1098/rstb.2016.0532.
6. Blair LJ, et al. The disease-associated chaperone FKBP51 impairs cognitive function by accelerating AMPA receptor recycling. eNeuro. 2019. https://doi.org/10.1523/ENEURO.0242-18.2019.
7. Rein T. Peptidylprolylisomerases, protein folders, or scaffolders? The example of FKBP51 and FKBP52. BioEssays. 2020;42:e1900250. https://doi.org/10.1002/bies.201900250.
8. Toneatto J, et al. Dynamic mitochondrial-nuclear redistribution of the immunophilin FKBP51 is regulated by the PKA signaling pathway to control gene expression during adipocyte differentiation. J Cell Sci. 2013;126:5357–68. https://doi.org/10.1242/jcs.125799.
9. Gallo LI, Lagadari M, Piwien-Pilipuk G, Galigniana MD. The 90-kDa heat-shock protein (Hsp90)-binding immunophilin FKBP51 is a mitochondrial protein that translocates to the nucleus to protect cells against oxidative stress. J Biol Chem. 2011;286:30152–60. https://doi.org/10.1074/jbc.M111.256610.
10. Sidibeh CO, et al. FKBP5 expression in human adipose tissue: potential role in glucose and lipid metabolism, adipogenesis and type 2 diabetes. Endocrine. 2018;62:116–28. https://doi.org/10.1007/s12020-018-1674-5.
11. Balsevich G, et al. Stress-responsive FKBP51 regulates AKT2-AS160 signaling and metabolic function. Nat Commun. 2017;8:1725. https://doi.org/10.1038/s41467-017-01783-y.
12. Pereira MJ, et al. FKBP5 expression in human adipose tissue increases following dexamethasone exposure and is associated with insulin resistance. Metabolism. 2014;63:1198–208. https://doi.org/10.1016/j.metabol.2014.05.015.
13. Stechschulte LA, et al. FKBP51 null mice are resistant to diet-induced obesity and the PPARgamma agonist rosiglitazone. Endocrinology. 2016;157:3888–900. https://doi.org/10.1210/en.2015-1996.
14. Stechschulte LA, et al. FKBP51 reciprocally regulates GRalpha and PPARgamma activation via the Akt-p38 pathway. Mol Endocrinol. 2014;28:1254–64. https://doi.org/10.1210/me.2014-1023.
15. Stechschulte LA, et al. FKBP51 controls cellular adipogenesis through p38 kinase-mediated phosphorylation of GRalpha and PPARgamma. Mol Endocrinol. 2014;28:1265–75. https://doi.org/10.1210/me.2014-1022.
16. Zhang L, et al. Loss of FKBP5 impedes adipocyte differentiation under both normoxia and hypoxic stress. Biochem Biophys Res Commun. 2017;485:761–7. https://doi.org/10.1016/j.bbrc.2017.02.126.
17. Radford BN, Han VKM. Evidence of increased hypoxia signaling in fetal liver from maternal nutrient restriction in mice. Pediatr Res. 2020;87:450–5. https://doi.org/10.1038/s41390-019-0447-z.
18. Kusumanchi P, et al. Stress-responsive gene FKBP5 mediates alcohol-induced liver injury through the hippo pathway and CXCL1 signaling. Hepatology. 2021. https://doi.org/10.1002/hep.31800.
19. Tatro ET, Everall IP, Kaul M, Achim CL. Modulation of glucocorticoid receptor nuclear translocation in neurons by immunophilins FKBP51 and FKBP52: implications for major depressive disorder. Brain Res. 2009;1286:1–12. https://doi.org/10.1016/j.brainres.2009.06.036.
20. Akiyama T, et al. Mitochondria-nucleus shuttling FK506-binding protein 51 interacts with TRAF proteins and facilitates the RIG-I-like receptor-mediated expression of type I IFN. PLoS ONE. 2014;9:e95992. https://doi.org/10.1371/journal.pone.0095992.
21. Toneatto J, Charo NL, Susperreguy S, Piwien-Pilipuk G. The dynamic mitochondria-nuclear redistribution of FKBP51 during the process of adipocyte differentiation is regulated by PKA. Medicina (B Aires). 2013;73:401–5.
22. Fichna M, et al. FKBP5 polymorphism is associated with insulin resistance in children and adolescents with obesity. Obes Res Clin Pract. 2018;12:62–70. https://doi.org/10.1016/j.orcp.2016.11.007.
23. Fichna M, et al. FKBP5 polymorphism is associated with insulin resistance in children and adolescents with obesity. Obes Res Clin Pract. 2016. https://doi.org/10.1016/j.orcp.2016.11.007.
24. Mitchell T, et al. Convergent mechanisms for dysregulation of mitochondrial quality control in metabolic disease: implications for mitochondrial therapeutics. Biochem Soc Trans. 2013;41:127–33. https://doi.org/10.1042/BST20120231.
25. Bohovych I, Chan SS, Khalimonchuk O. Mitochondrial protein quality control: the mechanisms guarding mitochondrial health. Antioxid Redox Signal. 2015;22:977–94. https://doi.org/10.1089/ars.2014.6199.
26. Pickles S, Vigie P, Youle RJ. Mitophagy and quality control mechanisms in mitochondrial maintenance. Curr Biol. 2018;28:R170–85. https://doi.org/10.1016/j.cub.2018.01.004.

27. Shi H, et al. Augmenter of liver regeneration protects against carbon tetrachloride-induced liver injury by promoting autophagy in mice. Oncotarget. 2017;8:12637–48. https://doi.org/10.18632/oncotarget.14478.

28. Gump JM, Thorburn A. Autophagy and apoptosis: what is the connection? Trends Cell Biol. 2011;21:387–92. https://doi.org/10.1016/j.tcb.2011.03.007.

29. McLelland GL, Soubannier V, Chen CX, McBride HM, Fon EA. Parkin and PINK1 function in a vesicular trafficking pathway regulating mitochondrial quality control. EMBO J. 2014;33:282–95. https://doi.org/10.1002/embj.201385902.

30. Endig J, et al. Acute liver injury after CCl4 administration is independent of Smad7 expression in myeloid cells. Int J Mol Sci. 2019. https://doi.org/10.3390/ijms20225528.

31. Dong S, et al. Mechanisms of CCl4-induced liver fibrosis with combined transcriptomic and proteomic analysis. J Toxicol Sci. 2016;41:561–72. https://doi.org/10.2131/jts.41.561.

32. Dai DF, et al. Congestive hepatic fibrosis score: a novel histologic assessment of clinical severity. Modern Pathol. 2014;27:1552–8. https://doi.org/10.1038/modpathol.2014.79.

33. Geisler F, Strazzabosco M. Emerging roles of Notch signaling in liver disease. Hepatology. 2015;61:382–92. https://doi.org/10.1002/hep.27268.

34. Qiu B, et al. FKBP51 modulates hippocampal size and function in post-translational regulation of Parkin. Cell Mol Life Sci. 2022;79:175. https://doi.org/10.1007/s00018-022-04167-8.

35. Boonying W, et al. Pink1 regulates FKBP5 interaction with AKT/PHLPP and protects neurons from neurotoxin stress induced by MPP(.). J Neurochem. 2019;150:312–29. https://doi.org/10.1111/jnc.14683.

36. Vergara D, et al. Cytoskeletal alterations and biomechanical properties of Parkin-mutant human primary fibroblasts. Cell Biochem Biophys. 2015;71:1395–404. https://doi.org/10.1007/s12013-014-0362-1.

37. Huynh DP, Scoles DR, Ho TH, Del Bigio MR, Pulst SM. Parkin is associated with actin filaments in neuronal and nonneural cells. Ann Neurol. 2000;48:737–44.

38. Xiao B, et al. Reactive oxygen species trigger Parkin/PINK1 pathway-dependent mitophagy by inducing mitochondrial recruitment of Parkin. J Biol Chem. 2017;292:16697–708. https://doi.org/10.1074/jbc.M117.787739.

39. Williams JA, Ni HM, Ding Y, Ding WX. Parkin regulates mitophagy and mitochondrial function to protect against alcohol-induced liver injury and steatosis in mice. Am J Physiol Gastrointest Liver Physiol. 2015;309:G324-340. https://doi.org/10.1152/ajpgi.00108.2015.

40. Vernucci E, et al. Mitophagy and oxidative stress in cancer and aging: focus on sirtuins and nanomaterials. Oxid Med Cell Longev. 2019;2019:6387357. https://doi.org/10.1155/2019/6387357.

41. Towers CG, et al. Mitochondrial-derived vesicles compensate for loss of LC3-mediated mitophagy. Develop Cell. 2021;56:2029-2042 e2025. https://doi.org/10.1016/j.devcel.2021.06.003.

42. Popov LD. Mitochondrial-derived vesicles: recent insights. J Cell Mol Med. 2022;26:3323–8. https://doi.org/10.1111/jcmm.17391.

43. Scarffe LA, Stevens DA, Dawson VL, Dawson TM. Parkin and PINK1: much more than mitophagy. Trends Neurosci. 2014;37:315–24. https://doi.org/10.1016/j.tins.2014.03.004.

44. Wei Y, Chiang WC, Sumpter R Jr, Mishra P, Levine B. Prohibitin 2 is an inner mitochondrial membrane mitophagy receptor. Cell. 2017;168:224-238. e210. https://doi.org/10.1016/j.cell.2016.11.042.

45. Ichimura Y, et al. Structural basis for sorting mechanism of p62 in selective autophagy. J Biol Chem. 2008;283:22847–57. https://doi.org/10.1074/jbc.M802182200.

46. Gaali S, et al. Selective inhibitors of the FK506-binding protein 51 by induced fit. Nat Chem Biol. 2015;11:33–7. https://doi.org/10.1038/nchembio.1699.

47. Konig L, et al. The selective FKBP51 inhibitor SAFit2 reduces alcohol consumption and reinstatement of conditioned alcohol effects in mice. Addict Biol. 2019. https://doi.org/10.1111/adb.12758.

48. Hartmann J, et al. Pharmacological inhibition of the psychiatric risk factor FKBP51 has anxiolytic properties. J Neurosci. 2015;35:9007–16. https://doi.org/10.1523/JNEUROSCI.4024-14.2015.

49. Masson MJ, Carpenter LD, Graf ML, Pohl LR. Pathogenic role of natural killer T and natural killer cells in acetaminophen-induced liver injury in

mice is dependent on the presence of dimethyl sulfoxide. Hepatology. 2008;48:889–97. https://doi.org/10.1002/hep.22400.

50. Loomba R, et al. Validation of serum test for advanced liver fibrosis in patients with nonalcoholic steatohepatitis. Clin Gastroenterol Hepatol. 2019;17:1867-1876 e1863. https://doi.org/10.1016/j.cgh.2018.11.004.

51. Romeo S, et al. Genetic variation in PNPLA3 confers susceptibility to nonalcoholic fatty liver disease. Nat Genet. 2008;40:1461–5. https://doi.org/10.1038/ng.257.

52. Sookoian S, Pirola CJ. Meta-analysis of the influence of I148M variant of patatin-like phospholipase domain containing 3 gene (PNPLA3) on the susceptibility and histological severity of nonalcoholic fatty liver disease. Hepatology. 2011;53:1883–94. https://doi.org/10.1002/hep.24283.

53. Chamoun Z, Vacca F, Parton RG, Gruenberg J. PNPLA3/adiponutrin functions in lipid droplet formation. Biol Cell. 2013;105:219–33. https://doi.org/10.1111/boc.201200036.

54. Zhang P, Verity MA, Reue K. Lipin-1 regulates autophagy clearance and intersects with statin drug effects in skeletal muscle. Cell Metab. 2014;20:267–79. https://doi.org/10.1016/j.cmet.2014.05.003.

55. Hong F, et al. The role of CYP2A5 in liver injury and fibrosis: chemical-specific difference. Naunyn Schmiedebergs Arch Pharmacol. 2016;389:33–43. https://doi.org/10.1007/s00210-015-1172-8.

56. Lu Y, Cederbaum AI. Cytochrome P450s and alcoholic liver disease. Curr Pharm Des. 2018;24:1502–17. https://doi.org/10.2174/1381612824666180410091511.

57. Andreola F, et al. Mouse liver CYP2C39 is a novel retinoic acid 4-hydroxylase. Its down-regulation offers a molecular basis for liver retinoid accumulation and fibrosis in aryl hydrocarbon receptor-null mice. J Biol Chem. 2004;279:3434–8. https://doi.org/10.1074/jbc.M305832200.

58. Rein T. Post-translational modifications and stress adaptation: the paradigm of FKBP51. Biochem Soc Trans. 2020;48:441–9. https://doi.org/10.1042/BST20190332.

59. Pei H, et al. FKBP51 affects cancer cell response to chemotherapy by negatively regulating Akt. Cancer Cell. 2009;16:259–66. https://doi.org/10.1016/j.ccr.2009.07.016.

60. Gassen NC, et al. SKP2 attenuates autophagy through Beclin1-ubiquitination and its inhibition reduces MERS-Coronavirus infection. Nat Commun. 2019;10:5770. https://doi.org/10.1038/s41467-019-13659-4.

61. Gassen NC, et al. FKBP51 inhibits GSK3beta and augments the effects of distinct psychotropic medications. Mol Psychiatry. 2016;21:277–89. https://doi.org/10.1038/mp.2015.38.

62. Baughman G, Wiederrecht GJ, Chang F, Martin MM, Bourgeois S. Tissue distribution and abundance of human FKBP51, and FK506-binding protein that can mediate calcineurin inhibition. Biochem Biophys Res Commun. 1997;232:437–43.

63. Deas E, Wood NW, Plun-Favreau H. Mitophagy and Parkinson's disease: the PINK1-parkin link. Biochim Biophys Acta. 1813;623–633:2011. https://doi.org/10.1016/j.bbamcr.2010.08.007.

64. Bertolin G, et al. The TOMM machinery is a molecular switch in PINK1 and PARK2/PARKIN-dependent mitochondrial clearance. Autophagy. 2013;9:1801–17. https://doi.org/10.4161/auto.25884.

65. Sarraf SA, et al. Landscape of the PARKIN-dependent ubiquitylome in response to mitochondrial depolarization. Nature. 2013;496:372–6. https://doi.org/10.1038/nature12043.

66. Sugiura A, McLelland GL, Fon EA, McBride HM. A new pathway for mitochondrial quality control: mitochondrial-derived vesicles. EMBO J. 2014;33:2142–56. https://doi.org/10.15252/embj.201488104.

67. Eiyama A, Okamoto K. PINK1/Parkin-mediated mitophagy in mammalian cells. Curr Opin Cell Biol. 2015;33:95–101. https://doi.org/10.1016/j.ceb.2015.01.002.

68. Fiesel FC, James ED, Hudec R, Springer W. Mitochondrial targeted HSP90 inhibitor Gamitrinib-TPP (G-TPP) induces PINK1/Parkin-dependent mitophagy. Oncotarget. 2017;8:106233–48. https://doi.org/10.18632/oncotarget.22287.

69. Bekhbat M, Rowson SA, Neigh GN. Checks and balances: the glucocorticoid receptor and NFkB in good times and bad. Front Neuroendocrinol. 2017;46:15–31. https://doi.org/10.1016/j.yfrne.2017.05.001.

70. Kastle M, et al. FKBP51 modulates steroid sensitivity and NFkappaB signalling: a novel anti-inflammatory drug target. Eur J Immunol. 2018;48:1904–14. https://doi.org/10.1002/eji.201847699.

Qiu *et al. Cell & Bioscience*   (2024) 14:1

Page 25 of 25

71. Weston CJ, Zimmermann HW, Adams DH. The role of myeloid-derived cells in the progression of liver disease. Front Immunol. 2019;10:893. https://doi.org/10.3389/fimmu.2019.00893.

72. Yang B, et al. Improved functional recovery to I/R injury in hearts from lipocalin-2 deficiency mice: restoration of mitochondrial function and phospholipids remodeling. Am J Transl Res. 2012;4:60–71.

73. Jin D, Zhang Y, Chen X. Lipocalin 2 deficiency inhibits cell proliferation, autophagy, and mitochondrial biogenesis in mouse embryonic cells. Mol Cell Biochem. 2011;351:165–72. https://doi.org/10.1007/s11010-011-0724-6.

74. Xu MJ, et al. Liver is the major source of elevated serum lipocalin-2 levels after bacterial infection or partial hepatectomy: a critical role for IL-6/STAT3. Hepatology. 2015;61:692–702. https://doi.org/10.1002/hep.27447.

75. Ciesielska A, Matyjek M, Kwiatkowska K. TLR4 and CD14 trafficking and its influence on LPS-induced pro-inflammatory signaling. Cell Mol Life Sci. 2021;78:1233–61. https://doi.org/10.1007/s00018-020-03656-y.

76. Zanoni I, et al. CD14 controls the LPS-induced endocytosis of Toll-like receptor 4. Cell. 2011;147:868–80. https://doi.org/10.1016/j.cell.2011.09.051.

77. Roy N, et al. Pattern recognition receptor CD14 gene polymorphisms in alcohol use disorder patients and its Influence on liver disease susceptibility. Front Immunol. 2022;13:975027. https://doi.org/10.3389/fimmu.2022.975027.

78. Al-Aalim AM, Al-Iedani AA, Hamad MA. Study of the effects of Escherichia coli lipopolysaccharide on innate immunity: the expression profile of TLR4 and CD14 genes in rat liver. Open Vet J. 2021;11:771–9. https://doi.org/10.5455/OVJ.2021.v11.i4.30.

79. Sequera C, Manzano S, Guerrero C, Porras A. How rap and its GEFs control liver physiology and cancer development. C3G alterations in human hepatocarcinoma. Hepat Oncol. 2018;5:1. https://doi.org/10.2217/hep-2017-0026.

80. Bristow JM, et al. The Rho-family GEF Asef2 activates Rac to modulate adhesion and actin dynamics and thereby regulate cell migration. J Cell Sci. 2009;122:4535–46. https://doi.org/10.1242/jcs.053728.

81. Mall DP, et al. Human FKBP5 negatively regulates transcription through inhibition of P-TEFb complex formation. Mol Cell Biol. 2022;42:e0034421. https://doi.org/10.1128/MCB.00344-21.

82. D'Arrigo P, et al. The splicing FK506-binding protein-51 isoform plays a role in glioblastoma resistance through programmed cell death ligand-1 expression regulation. Cell Death Discov. 2019;5:137. https://doi.org/10.1038/s41420-019-0216-0.

83. Romano S, et al. FKBP51s signature in peripheral blood mononuclear cells of melanoma patients as a possible predictive factor for immunotherapy. Cancer Immunol Immunother. 2017;66:1143–51. https://doi.org/10.1007/s00262-017-2004-0.

84. Li L, Lou Z, Wang L. The role of FKBP5 in cancer aetiology and chemoresistance. Br J Cancer. 2011;104:19–23. https://doi.org/10.1038/sj.bjc.6606014.

85. Yong W, et al. Essential role for Co-chaperone Fkbp52 but not Fkbp51 in androgen receptor-mediated signaling and physiology. J Biol Chem. 2007;282:5026–36. https://doi.org/10.1074/jbc.M609360200.

86. Yang JH, et al. Neoagarooligosaccharide protects against hepatic fibrosis via inhibition of TGF-beta/Smad signaling pathway. Int J Mol Sci. 2021. https://doi.org/10.3390/ijms22042041.

87. Spence JP, et al. Estrogen-dependent upregulation of Adcyap1r1 expression in nucleus accumbens is associated with genetic predisposition of sex-specific QTL for alcohol consumption on rat chromosome 4. Front Genet. 2018;9:513. https://doi.org/10.3389/fgene.2018.00513.

88. Trapnell C, Pachter L, Salzberg SL. TopHat: discovering splice junctions with RNA-Seq. Bioinformatics. 2009;25:1105–11. https://doi.org/10.1093/bioinformatics/btp120.

89. Benjamini Y, Hochberg Y. Controlling the false discovery rate: a practical and powerful approach to multiple testing. J Royal Stat Soc (B). 1995;57:289–90.

90. Bolte S, Cordelieres FP. A guided tour into subcellular colocalization analysis in light microscopy. J Microsc. 2006;224:213–32. https://doi.org/10.1111/j.1365-2818.2006.01706.x.

91. Cao Y, et al. Miro2 regulates inter-mitochondrial communication in the heart and protects against TAC-induced cardiac dysfunction. Circ Res. 2019;125:728–43. https://doi.org/10.1161/CIRCRESAHA.119.315432.

92. Qiu B, et al. CART attenuates endoplasmic reticulum stress response induced by cerebral ischemia and reperfusion through upregulating BDNF synthesis and secretion. Biochem Biophys Res Commun. 2013;436:655–9. https://doi.org/10.1016/j.bbrc.2013.05.142.

93. Qiu B, et al. NPY deletion in an alcohol non-preferring rat model elicits differential effects on alcohol consumption and body weight. J Genet Genomics Yi chuan xue bao. 2016;43:421–30. https://doi.org/10.1016/j.jgg.2016.04.010.

94. Qiu B, et al. Loss of FKBP5 affects neuron synaptic plasticity: an electrophysiology insight. Neuroscience. 2019;402:23–36. https://doi.org/10.1016/j.neuroscience.2019.01.021.

95. Feng X, Sippel C, Bracher A, Hausch F. Structure–affinity relationship analysis of selective FKBP51 ligands. J Med Chem. 2015;58:7796–806. https://doi.org/10.1021/acs.jmedchem.5b00785.

Publisher's Note

Springer Nature remains neutral with regard to jurisdictional claims in published maps and institutional affiliations.